

DFT-based Global Optimization Of Sub-nanometre Ni-Pd Clusters

Alejandra Granja-DelRío,^{*,†} Heider A. Abdulhussein,^{‡,¶} and Roy L. Johnston^{*,¶}

[†] *Departamento de Física Teórica, Atómica y Óptica, Universidad de Valladolid, 47011
Valladolid, Spain*

[‡] *Department of Chemistry, College of Science, University of Kufa, Najaf, Iraq*

[¶] *School of Chemistry, University of Birmingham, Edgbaston, Birmingham, B15 2TT, UK*

E-mail: agranjadelrio@gmail.com; r.l.johnston@bham.ac.uk

Abstract

The Mexican Enhanced Genetic Algorithm (MEGA) has been used to study the structural and energetic properties of Pd, Ni and Ni-Pd nanocluster structures with 3-10 atoms. Density functional theory (DFT) calculations have been performed to investigate the structural behaviour, spin magnetic moments and stability as a function of cluster size and composition. Various stability criteria (e.g binding energies, second differences in energy and mixing/excess energies) have been used to evaluate the energetics, structures and tendency to segregation in sub-nanometre Ni-Pd clusters. The ability of the approach in searching for global minima (i.e. the lowest energy isomers) has been assessed using a systematic homotop search of mono-substituted clusters and the preferred doping sites.

Introduction

Catalysis is of critical importance in many industrial processes. Recently, there has been significant interest in catalysis by single metal atoms and small sub-nanometre metal clusters supported on oxides or carbon surfaces.¹⁻¹¹ One important example is their use in hydrogen storage, since hydrogen is an energy carrier and is a promising replacement for fossil fuels.¹²⁻²⁰

Transition metal clusters (TMCs) show special catalytic, optical, magnetic, electronic and geometric properties, as they do not behave as either atoms or solids. Since cluster properties evolve with size, designed clusters with tailored properties are promising avenues of current research. TM nanoparticles and sub-nanometre clusters have been studied for potential use in many different applications. In addition, there is increasing interest in bimetallic clusters, also known as “nanoalloys”. This interest is due to the important potential of being able to manipulate the properties of the clusters by varying their composition, as well as size, for specific technical applications, for example, in the recording industry and in future electronics. Magnetism is an important property of many clusters. One of the most important

characteristics related to magnetic properties is the geometrical structure of the material, since the properties of $3d$ electrons are sensitive to changes in the position of the atoms within the system. The properties of nanoalloys can be tuned in three ways: (i) changing their size and shape; (ii) changing their elemental composition; and (iii) changing their chemical ordering (i.e. how the component metals are distributed within the cluster). It is known that sub-nanometre clusters have properties that are generally different from the bulk and do not always scale linearly with size, i.e. they are in the size regime where “each atom counts”, paraphrasing the title of a paper of Heiz.²¹ Nanoalloys can also show physical and chemical properties that are distinct from their component metals. In the catalysis field, synergistic interactions between metals can give rise to catalysts with greater activity, selectivity and/or stability, compared to pure metal nanocatalysts.²² Changing the composition and chemical order of the nanoalloys can enhance these properties,^{23,24} for example by modifying activation energy barriers.²⁵ Thus, studying the structures and properties (spin magnetic moment, optics, activation energies, composition...) of these clusters is a vital step towards understanding their role in catalysis.²⁶⁻⁴¹ Recent developments in computational methods and computer hardware enables the prediction of novel candidates for nanocatalysts for a variety of chemical processes.

The fact that catalysts are widely used in industry has motivated experiments on new nanoscale materials. This is in part driven by economic considerations. For example, it is known that gold, platinum and platinum-based nanoparticles exhibit exceptional catalytic properties,^{42,43} but applications are generally limited due to the high cost of these elements. This has motivated researchers to look for alternative, cheaper metals or alloys to replace Pt and other precious metals, lowering costs while maintaining (or even improving) the catalytic performance.⁴⁴⁻⁵⁰ The greater abundance of Pd has made this element a good substitute for Pt⁴⁵ and several applications (in diverse technological fields) have been investigated using Pd, due to its interesting magnetic, electronic and catalytic properties.^{17,25,42,51-54} However, further cost savings are possible by alloying Pd with lower cost metals such as Co, Cu and

Ni.

The improvement of material properties and the possible discovery of new properties is an important driving force for the design of novel nanomaterials and nanoalloys. The Ni-Pd bimetallic system, for example, shows enhanced electrocatalytic properties for the oxygen reduction reaction (ORR)^{27,28,55} and this bimetallic system is widely used as cathode electrocatalysts for alkaline fuel cells.^{56,57} Nieves-Torres et al. have compared Ni-Pd with pure Pd nanoparticles and the bimetallic clusters showed improved catalytic activity and/or selectivity.⁵⁸ Son et al. found that these nanoparticles can be reused several times without losing catalytic activity.^{30,59-61}

Gas-phase sub-nanometre clusters are simplified models that can be used to test the suitability of these systems for specific catalytic applications using computational studies, in a reasonable amount of computer time, before dealing with more complex, larger systems. Theoretical studies have shown that depositing pure Ni and Pd clusters on different surfaces^{14,62,63} or adsorbing molecules onto the pure clusters can induce structural changes, changes in the magnetic and electronic properties and/or changes in the stereochemical properties.^{26,64-68}

The DFT-based Birmingham Parallel Genetic Algorithm (BPGA) and Mexican Enhanced Genetic Algorithm (MEGA) have been successfully applied to search for the lowest energy isomers for a variety of mono- and bimetallic nanoclusters.⁶⁹⁻⁷²

The aim of this work is to study the structural properties (size, order/placement of the atoms in the nanoalloy, energetics, spin magnetic moments) of binary Ni-Pd nanoalloys, including a comparison with pure clusters. Employing the MEGA-DFT code, the global minima for Ni, Pd and Ni-Pd clusters with 3-10 atoms have been calculated (including all compositions for the nanoalloys). The localized behaviour of unfilled *3d* electrons of nickel clusters results in enormous complexity and dominate most of their properties.

There have been several first-principles calculations for pure Ni clusters⁷³⁻⁷⁵ and for bimetallic Ni-clusters,^{76,77} but there have been only few for Ni-Pd nanoalloys.^{78,79} In this

context, we present here a comprehensive theoretical study of the physico-chemical properties of Ni-Pd clusters, including a comparison to their pure clusters, investigating the effect of their alloying on the structures, stabilities and spin magnetic moments. In Section 2, we describe the computational method adopted. In Section 3, we present and discuss our results and our conclusions are presented in Section 4.

Computational Details

Calculations were performed with the Mexican Enhanced Genetic Algorithm (MEGA)^{72,80} using an interface to the Vienna Ab-initio Simulation Package (VASP)⁸¹⁻⁸⁴ for the global optimization of Ni-Pd nanoalloys and the pure clusters. MEGA is a genetic algorithm for the structural characterization of nanoparticles and is written in object-oriented Python. It is based on the Birmingham Parallel Genetic Algorithm (BPGA)^{41,85} and includes many new features to improve its functionality and performance, like an error-proof corrector for short distances between atoms, more mutations types and the inclusion of structural (as well as energetic) comparisons to help maintain population diversity. Both BPGA and MEGA, are capable of carrying out independent and parallel relaxations synchronized with a global database or pool, which stores the atomic coordinates and energies of the current most stable cluster configurations for a given nuclearity and elemental composition.

In MEGA the initial pool population is formed by generating a number (in our case 10) of random isomers. These random structures are then geometrically relaxed by local DFT energy minimization, which is performed in parallel on multiple processors.⁷² The genetic algorithm crossover and mutation operators are applied to members of the pool in order to generate new structures. For crossover, a pair of clusters are chosen from the pool using a weighted roulette-wheel selection⁴¹ and they undergo crossover using a variant of Deaven and Ho phenotypic cut-and-splice method to generate a single offspring.⁸⁶ Different mutation operations, including “move”, “rotate”, “twist” and “atom inversion”, are used in

MEGA and the relative probability of each type of mutation can be predefined. “Move” mutation displaces 25% of total number of atoms of cluster shifting their coordinates by a certain value, x , ($-r_a \leq x \leq +r_a$), where r_a is the atomic radius. “Rotate” mutation rotates 25% of the cluster atoms rigidly around an axis passing through the centre of mass and directed randomly. Similar to “rotate” mutation, “twist” mutation also rotates the cluster atoms rigidly but 50% of the atoms are rotated through a random angle relative to the other half of the cluster, retaining the same geometry within each half. “Atom inversion” mutation inverts one atom through the cluster centre of mass from one side to the other. This operation can be simply achieved by changing the signs of the coordinates of the relevant atom. The new structures generated by crossover and mutation are subsequently energy minimized at the DFT level and compared energetically with the existing members of the pool, such that the highest energy isomers are replaced with lower energy offspring and mutants. In our case the mutation rate was 30% of the pool size (3 out of 10 pool structures mutated) and the mating rate was 70% (7 pairs undergo crossover).

Accordingly, 400 structures are locally minimized in each run. The convergence is achieved when energy of the lowest-energy isomers in two successive runs is within 10^{-4} eV. Therefore, the isomers that compete energetically to form the final pool (lowest-energy 10 isomers) is more than 1000 structures in total for each composition of a given size.

Energy calculations and local minimizations are performed with the VASP package,⁸¹⁻⁸⁴ using the generalized gradient approximation (GGA) Perdew-Burke-Erzenhof (PBE) exchange and correlation functional⁸⁷ and Projected Augmented Wave (PAW) pseudopotentials.⁸⁸ The energy cut-off for the plane waves is 400 eV. Gamma-point DFT calculations are performed with spin polarization so the multiplicities of the clusters can be obtained.

To elucidate the multiplicity of all the MEGA-DFT global minima obtained with VASP, spin-polarized reoptimizations are carried out with GAUSSIAN09,⁸⁹ using the ω B97XD exchange-correlation functional^{90,91} and def2TZVPP^{92,93} basis set for all the reminimisations and single-point energy calculations. The ω B97XD/def2TZVPP approach has been

employed to find out the optimal spin state for their compromising between accuracy and computational resources, as evident by Raju *et al.*⁹⁴ for such metallic systems.

Ionization energies (I) and electron affinities (A) are calculated for all nanoalloys, using Koopman's approximation:⁹⁵

$$I = -E_{HOMO} \quad (1)$$

$$A = -E_{LUMO} \quad (2)$$

I and A are used to calculate the conceptual DFT-based descriptors: electronegativity (χ), global hardness (η), and electrophilicity index (ω), which are given by:

$$\chi = -\mu = \frac{I + A}{2} \quad (3)$$

where μ represents the chemical potential of the system.

$$\eta = \frac{I - A}{2} \quad (4)$$

$$\omega = \frac{\mu^2}{2\eta} \quad (5)$$

We have studied the stability of the nanoclusters. For pure Ni and Pd clusters, the stability of each cluster, relative to its neighbours, is indicated by the second difference in energy (6):

$$\Delta_2 E = E_{(A_{N+1})} + E_{(A_{N-1})} - 2E_{(A_N)} \quad (6)$$

where A is Ni or Pd, $E_{(A_N)}$ corresponds to the total energy of the N -atom cluster and $E_{(A_{N+1})}$ and $E_{(A_{N-1})}$ are the energies of the neighbouring clusters, with one more and one less atom, respectively.

The average binding energy per atom E_b is given by (7):

$$E_b = \frac{-1}{N} [E_{(\text{Ni}_m\text{Pd}_n)} - mE_{(\text{Ni})} - nE_{(\text{Pd})}] \quad (7)$$

where m , n , $E_{(\text{Ni})}$ and $E_{(\text{Pd})}$ are the number of Ni and Pd atoms and the energies of a single Ni or Pd atom, respectively, and N is the total number of atoms ($N = m + n$).

The effect of mixing Pd with Ni atoms in nanoalloys can be evaluated by calculating the mixing (or excess) energy Δ , given by (8):

$$\Delta = E_{(\text{Ni}_m\text{Pd}_n)} - m \frac{E_{(\text{Ni}_N)}}{N} - n \frac{E_{(\text{Pd}_N)}}{N} \quad (8)$$

where $E_{(\text{Ni}_m\text{Pd}_n)}$ is the total energy of the nanoalloy and $E_{(\text{Ni}_N)}$ and $E_{(\text{Pd}_N)}$ are the energies of the pure Ni and Pd clusters with the same total number of atoms as Ni_mPd_n .

For a given cluster size (N) and composition (m , n), the relative energies of a homotop h_i (inequivalent permutational isomer^{39,96}) of the lowest energy structure (the global minimum, GM) are defined as:

$$\Delta E(h_i) = E(h_i) - E(GM) \quad (9)$$

Results and discussion

Structures

To check the validity of the computational method for the study of the bimetallic Ni-Pd nanoalloys, the binding energies (BEs) of Pd and Ni dimers were calculated as 0.67 and 1.47 eV per atom, respectively. The bond length of the Pd dimer is 2.47 Å and for the Ni dimer it is 2.08 Å. The obtained results for the Pd dimer are in agreement with experimental⁹⁷ and theoretical results,⁵² as listed in Table 1. However, the binding energies obtained for the Ni dimer present a little discrepancy with experimental ones,^{98,99} as listed in Table 2. The BE of the Ni-Pd dimer (1.13 eV per atom) lies between those of Pd₂ and Ni₂ and the

bond length is 2.23 Å. Thus, Ni_mPd_n nanolloy properties are expected to lie between those of pure palladium and nickel clusters.

Table 1: Comparison of DFT computational results for Pd₂ cluster with experimental and theoretical data

| Authors | Binding Energies (BE) eV/atom | Distance Å |
|--|-------------------------------|------------|
| Huber <i>et al.</i> ⁹⁷ (experimental) | 0.698 | 2.48 |
| Mu <i>et al.</i> ⁵² (theoretical) | 0.603 | 2.486 |
| Ours | 0.67 | 2.47 |

Table 2: Comparison of DFT computational results for Ni₂ cluster with experimental and theoretical data

| Authors | Binding Energies (BE) eV/atom | Distance Å |
|---|-------------------------------|------------|
| Morse <i>et al.</i> ⁹⁸ (experimental) | 1.034 | 2.155 |
| Chen <i>et al.</i> ¹⁰⁰ (theoretical) | 1.43 | 2.12 |
| Castro <i>et al.</i> ¹⁰¹ (theoretical) | 1.74 | 2.1 |
| Ours | 1.47 | 2.08 |

Pd clusters

The putative global minima for pure Pd clusters, $3 \leq N \leq 10$, are shown in Fig. 1 and their binding energies per atom, structures, point groups and spin magnetic moments (SMM) are listed in Table 3.

As reported previously, Pd clusters have 3D motifs for sizes $4 \leq N \leq 10$ showing compact structures as lowest-energy configurations.^{52,102,103} The ground state structure of the Pd trimer is a C_{2v} isosceles triangle with a spin magnetic moment of 2 μ_B which is consistent with DFT results reported by other researchers.¹⁰⁴

For $N = 4 - 10$ clusters, the geometries and spin magnetic moments for the ground state are in full agreement with the gas-phase Pd clusters previously reported by Zanti *et al.*¹⁰³ and Aguilera-Granja *et al.*¹⁰⁵ However, for $N = 9$, we have found the spin magnetic moment to be almost degenerate in energy, with an energy difference of only 5 meV between the triplet and the quintet (more stable states).

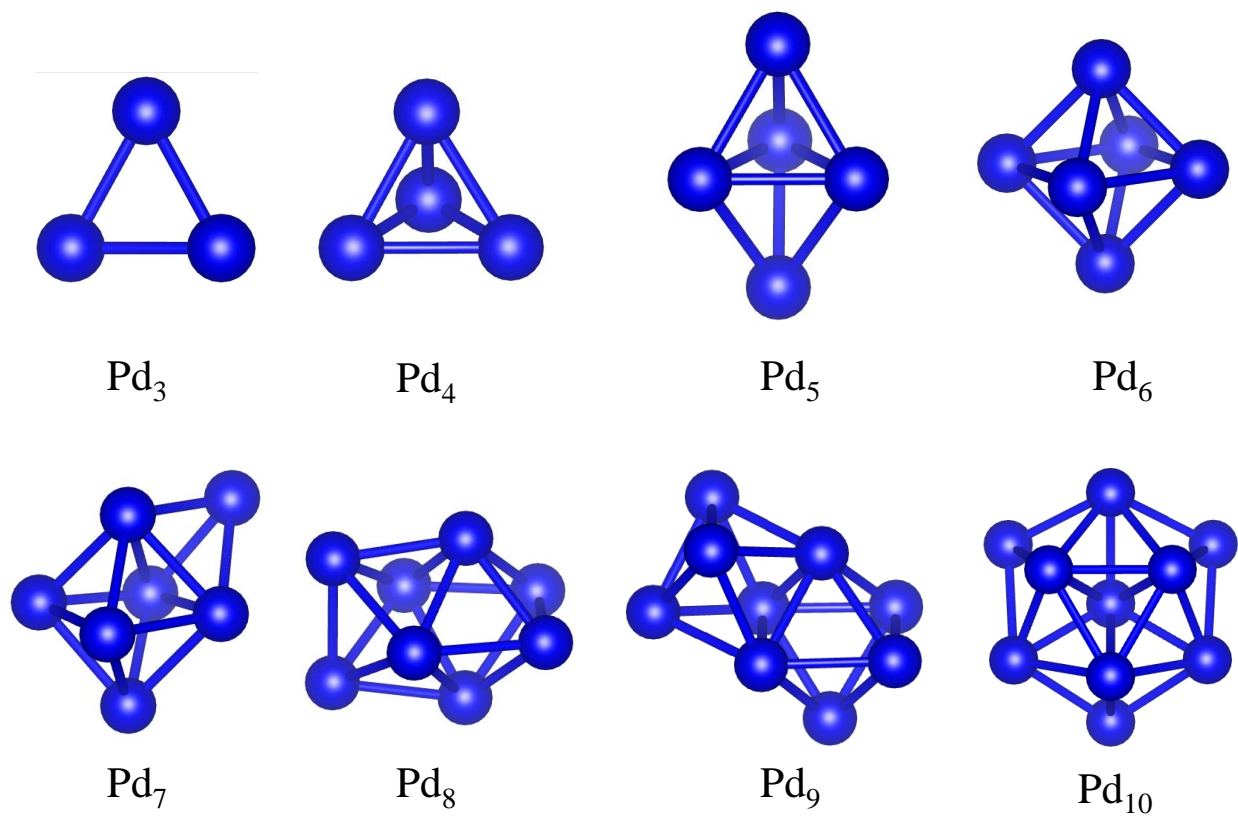


Figure 1: Putative global minimum structures for Pd_N clusters, $N = 3 - 10$.

Table 3: Structures, point groups and Pd-Pd average distances (AD) for Pd_N clusters, N = 3 – 10

| Composition | Structure | Point Group | Pd-Pd AD / Å |
|------------------|---------------------------|-----------------|--------------|
| Pd ₃ | Isosceles triangle | C _{2v} | 2.49 |
| Pd ₄ | Tetrahedron | T _d | 2.59 |
| Pd ₅ | Trigonal bipyramid | D _{3h} | 2.63 |
| Pd ₆ | Octahedron | O _h | 2.64 |
| Pd ₇ | Capped octahedron | C _{3v} | 2.68 |
| Pd ₈ | Dodecahedron | D _{2d} | 2.67 |
| Pd ₉ | Face-sharing bioctahedron | D _{3h} | 2.63 |
| Pd ₁₀ | Icosahedral fragment | C _{3v} | 2.64 |

Ni clusters

The lowest energy structures obtained from global optimization for pure Ni_N clusters ($3 \leq N \leq 10$) are shown in Fig. 2 and their binding energies per atom, structures, point groups and spin magnetic moments are collected in Table 4. The structures in this size range show 3D configurations, as previously reported.^{63,106–109} The spin magnetic moments of the Ni clusters are larger than the bulk value $0.6 \mu_B$. The magnitude of spin magnetic moments fluctuates for clusters smaller than $N = 8$ ¹⁰⁷ as shown in Fig. 3. From $N = 8$ a linear decrease has been reported on the basis of theoretical and experimental results.^{107,110} However, some differences have been observed for the Ni₇ and Ni₈ in ref.¹⁰⁶ and the Ni₇ and Ni₁₀ in ref.⁶³ Nevertheless, the Ni₇ structure is the same as reported by Aguilera-Granja *et al.*¹⁰⁸ but the spin magnetic moment is different. The discrepancy in the spin magnetic moment may be due to different methods of calculation or to the different initial structures.

The most stable isomer of Ni₃ is identified as a C_{2v} isosceles triangle with a spin magnetic moment of $4 \mu_B$. The structures for $4 \leq N \leq 10$ have 3D geometries. Ni₄ is tetrahedron (T_d)

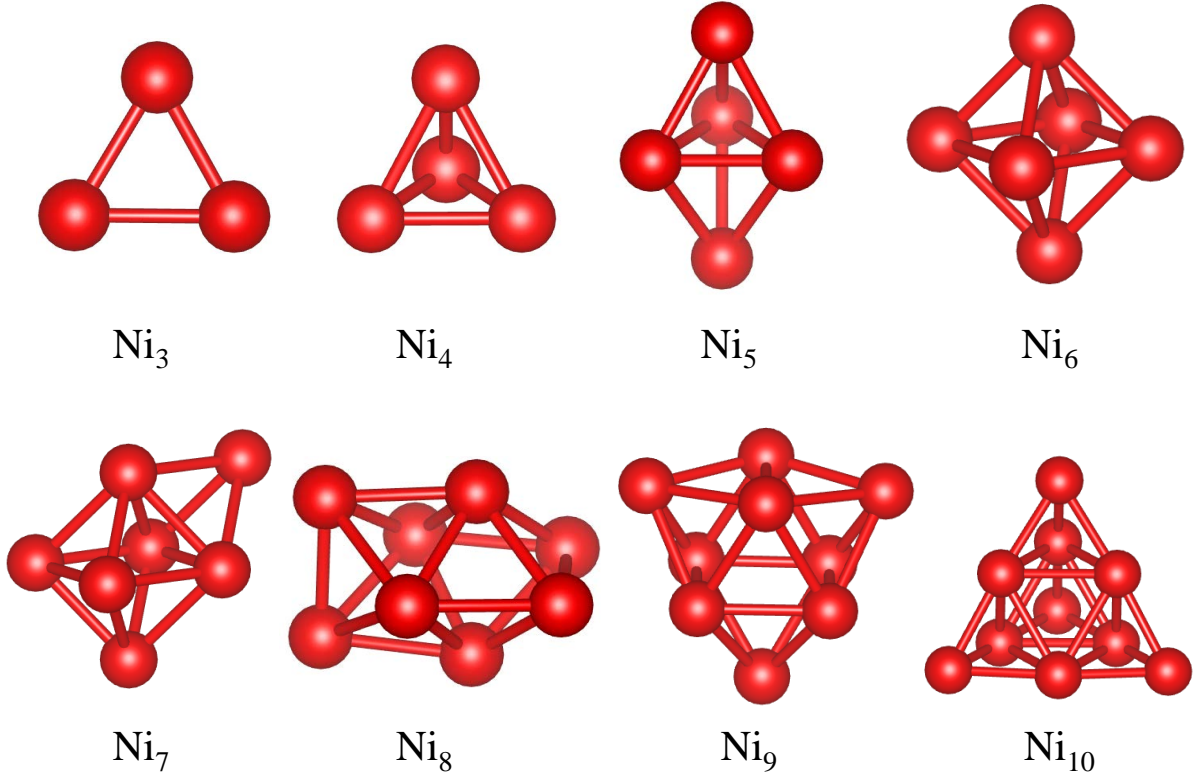


Figure 2: Putative global minimum structures for Ni_N clusters, $N = 3 - 10$.

Table 4: Structures, point groups and Ni-Ni average distances (AD) for Ni_N clusters, $N = 3 - 10$

| Composition | Structure | Point Group | Ni-Ni AD / Å |
|------------------|--------------------------|-------------|--------------|
| Ni_3 | Isosceles triangle | C_{2v} | 2.17 |
| Ni_4 | Tetrahedron | T_d | 2.30 |
| Ni_5 | Trigonal bipyramid | D_{3h} | 2.31 |
| Ni_6 | Octahedron | O_h | 2.31 |
| Ni_7 | Capped octahedron | C_{3v} | 2.32 |
| Ni_8 | Dodecahedron | D_{2d} | 2.35 |
| Ni_9 | Tricapped trigonal prism | D_{3h} | 2.31 |
| Ni_{10} | Tetra-capped-octahedron | T_d | 2.33 |

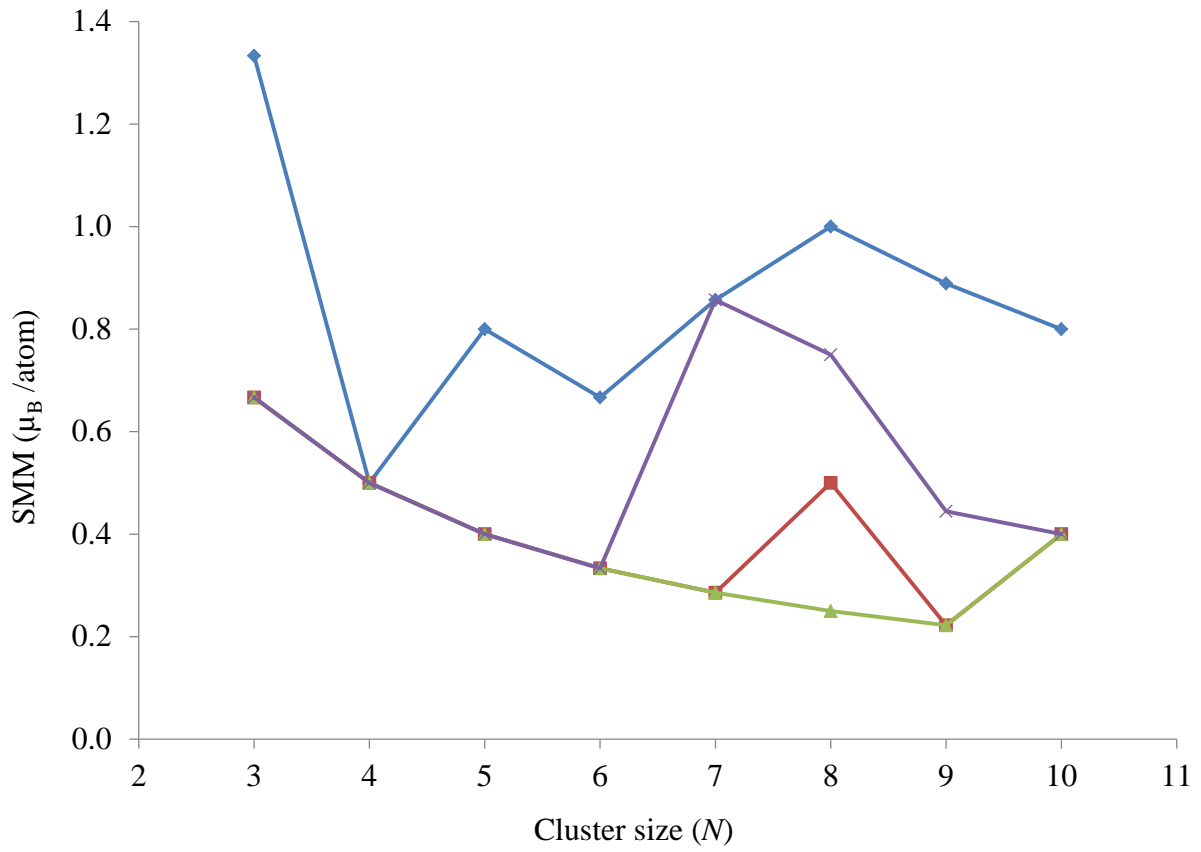


Figure 3: Spin magnetic moments (SMM) per atom of Ni_N (blue), Pd_N (red), Ni_1Pd_{N-1} (green) and $Ni_{N-1}Pd_1$ (mauve) clusters as a function of the cluster size for $N = 3 - 10$.

with a spin magnetic moment of $2 \mu_B$.¹⁰⁹ These findings agree with those reported by Xie *et al.*¹¹¹ For the Ni pentamer, a trigonal bipyramid (D_{3h}) has been found as the GM energy structure, with a spin magnetic moment of $4 \mu_B$. The structure and magnetic moment are the same as reported by Xie *et al.*¹⁰⁹

Ni₆ is found to be an octahedron (with full O_h symmetry), which is entirely consistent with previous theoretical calculations,^{63,109} and a spin magnetic moment of $4 \mu_B$. Ni₇ has an additional Ni atom capping a face of the octahedron (C_{3v} symmetry) as reported by Aguilera-Granja *et al.*,¹⁰⁸ and a spin magnetic moment of $6 \mu_B$. Xie *et al.* and Nayak *et al.*⁷³ suggested that the capped octahedron and the pentagonal bipyramid (with D_{5h} symmetry) are nearly degenerate isomers. We found the pentagonal bipyramid to lie approximately 0.16 eV higher in energy than the capped octahedron. This is the reason why some researchers have reported the pentagonal bipyramid^{63,109} as the GM and others the capped octahedron.¹⁰⁸

The lowest energy structure for Ni₈ is found to be a dodecahedron (D_{2d}) and the Ni₉ cluster "has a tricapped trigonal prism structure (D_{3h} symmetry), in agreement with Xie *et al.*¹⁰⁹ and similar to the results reported by Wang *et al.*¹¹¹ for Ni₈Mn. We have obtained $8 \mu_B$ for both Ni₈ and Ni₉, in agreement with results obtained by Xie *et al.*¹⁰⁹

Finally, we have studied Ni₁₀, which is found to be a tetra-capped octahedron (T_d symmetry) with a spin magnetic moment of $8 \mu_B$, in agreement with the results of Xie *et al.*¹⁰⁹

Nickel-Palladium clusters

The global minima for all compositions of Ni_{*m*}Pd_{*n*} in the gas-phase, $3 \leq N \leq 10$, are shown in Figs. 4, 5 and 6 and their binding energies per atom, structures, point groups and spin magnetic moments are collected in Table 5. In nanoalloys, there is an increase in difficulty of identifying the global minimum structure, due to the presence of "homotops" (isomers differing only in the distribution of the component metal atoms).⁹⁶

First, we have studied all the lowest structures of Ni₁Pd_{*n*} $n = 2 - 9$. For $n = 2 - 9$. Doping one Ni atom into the pure Pd clusters yields geometries which are similar to the

pure Pd clusters. The Ni atom occupies a high-connectivity vertex, maximizing the number of Ni-Pd bonds, which are stronger than Pd-Pd bonds, as shown above for the dimers.

The Ni structures, described in Ni clusters section, remain the GM when they are doped with a single Pd atom except for Ni_5Pd_1 , which adopts the structure of an incomplete pentagonal bipyramid (iPB), which is equivalent to a bicapped tetrahedron. The Pd atoms are located in low-connectivity sites, maximizing the number of the stronger Ni-Ni bonds and thereby increasing the cluster stability.

We have subsequently investigated all possible nanoalloy compositions for all the sizes $4 \leq N \leq 10$. Ni_3Pd_1 , Ni_2Pd_2 and Ni_1Pd_3 are all tetrahedra, with spin magnetic moments of $2 \mu_B$. The gas-phase global minima for Ni_1Pd_4 , Ni_2Pd_3 , Ni_3Pd_2 and Ni_4Pd_1 are all trigonal bipyramids, with spin magnetic moments of $2 \mu_B$.

The lowest energy structure for Ni_1Pd_5 is an octahedron and the other clusters with $N = 6$ (Ni_2Pd_4 , Ni_3Pd_3 , Ni_4Pd_2 and Ni_5Pd_1) are bicapped tetrahedra (incomplete pentagonal bipyramids, iPB). The spin magnetic moments for these clusters are $2 \mu_B$, except for Ni_4Pd_2 ($4 \mu_B$).

For $N = 7$, the capped octahedron is the GM for Ni_1Pd_6 , Ni_3Pd_4 and Ni_6Pd_1 . For Ni_4Pd_3 and Ni_5Pd_2 the GM is a pentagonal bipyramid and for Ni_2Pd_5 the GM consists of two fused trigonal bipyramids and is only 5 meV lower than the capped octahedron for the same composition (see Fig. 7). The spin magnetic moments are $2 \mu_B$ for all the structures except for Ni_3Pd_4 and Ni_6Pd_1 , which have values of 4 and $6 \mu_B$, respectively.

For $N = 8$, all the clusters have the same dodecahedral structure, except for Ni_3Pd_5 , which is a fused octahedron with a square pyramid, and Ni_5Pd_3 and Ni_6Pd_2 , which both have bicapped octahedral structures (with the caps in the “meta-” position). The spin magnetic moments for $N = 8$ increase with increasing Ni content. For Ni_1Pd_7 , Ni_2Pd_6 and Ni_3Pd_5 the spin magnetic moments are $2 \mu_B$, while Ni_4Pd_4 and Ni_5Pd_3 have $4 \mu_B$ and the spin magnetic moments for Ni_6Pd_2 and Ni_7Pd_1 are $6 \mu_B$.

Global minima for $\text{Ni}_1\text{Pd}_8 - \text{Ni}_3\text{Pd}_6$ are face-sharing bioctahedral structures, while Ni_5Pd_4

–Ni₈Pd₁ are tricapped trigonal prisms. Ni₄Pd₅ has a structure composed of two fused trigonal prisms, capped on one of the square faces. The spin magnetic moments are 2 μ_B for all the structures except Ni₈Pd₁, Ni₂Pd₇ and Ni₇Pd₂ which have values of 4, 4 and 6 μ_B respectively.

Finally, we have investigated the nanoalloys with $N = 10$. The GM for Ni₉Pd₁ – Ni₆Pd₄ are tetracapped octahedral structures, while Ni₅Pd₅ – Ni₂Pd₈ are complex polytetrahedral structures. Ni₁Pd₉ is a fragment of a 13-atom centred icosahedron. Most of the structures have spin magnetic moments of 4 μ_B , except Ni₈Pd₂ and Ni₁Pd₉ (2 μ_B). Ni₃Pd₇ (6 μ_B) and Ni₆Pd₄ (8 μ_B).

Although the magnetism occurs due to the presence of unpaired spins, the bonding states of small and bulk atomic clusters are unlike. The small clusters generally show much higher spin states than their bulk states.^{112,113} The bonding states for the bulk systems can be explained depending on the number of unpaired electron in the d orbital. However, the magnetism of small atomic clusters can be easily affected by the size of the cluster and compositions.¹¹⁴ Looking at the trends of the magnetic properties as a function of the interatomic distance and geometries of Ni-Pd clusters, the number of unpaired spins are shown to be preserved by having large interatomic distances and thus results in a high magnetic moment, as seen for Ni₇ (6 μ_B), $N = 8 - 10$ Ni_N clusters (8 μ_B), Ni₆Pd₁ (6 μ_B), Ni₆Pd₂ (6 μ_B), Ni₇Pd₁ (6 μ_B), Ni₇Pd₂ (6 μ_B), Ni₃Pd₇ (6 μ_B), and Ni₆Pd₄ (8 μ_B). This explains why the magnetic moment is relatively higher for the larger Ni-Pd clusters. For clusters of the same size, the difference of structures and interatomic distances play a crucial role in changing their magnetism. For instance, Pd (a closed $4d$ shell metal) doping can clearly distort the symmetry or alter the structure of pure Ni clusters and then results in changing of the magnetic moment, as seen for all our mono-Pd doped Ni clusters except for size $N = 7$. Such observation was previously proven for nickel clusters by Reddy and co-workers⁷⁴ where large magnetic moment is resulted by the low coordination and large interatomic distance. In conclusion, magnetism of such systems can decrease when the

overlap between neighbour atoms are higher (i.e. increase the overlap of electron pairing).

Table 5: Structures, point groups, Ni-Ni, Pd-Pd and Ni-Pd average distances (AD) for all compositions of Ni_mPd_n clusters, $N = m + n = 3 - 9$

| Composition | Structure | Point Group | Ni-Ni AD / Å | Ni-Pd AD / Å | Pd-Pd AD / Å |
|--------------------------|---|-------------|--------------|--------------|--------------|
| Ni_1Pd_2 | Isosceles triangle | C_{2v} | | 2.32 | 2.60 |
| Ni_2Pd_1 | Isosceles triangle | C_{2v} | 2.16 | 2.38 | |
| Ni_1Pd_3 | Tetrahedron | C_{3v} | | 2.37 | 2.67 |
| Ni_2Pd_2 | Tetrahedron | C_{2v} | 2.25 | 2.42 | 2.74 |
| Ni_3Pd_1 | Tetrahedron | C_{3v} | 2.27 | 2.46 | |
| Ni_1Pd_4 | Trigonal bipyramid | C_{2v} | | 2.42 | 2.65 |
| Ni_2Pd_3 | Trigonal bipyramid | D_{3h} | 2.27 | 2.44 | 2.67 |
| Ni_3Pd_2 | Trigonal bipyramid | C_{2v} | 2.46 | 2.27 | |
| Ni_4Pd_1 | Trigonal bipyramid | C_{2v} | 2.29 | 2.47 | |
| Ni_1Pd_5 | Octahedron | C_{4v} | | 2.44 | 2.69 |
| Ni_2Pd_4 | Bicapped tetrahedron | C_{2v} | 2.27 | 2.47 | 2.66 |
| Ni_3Pd_3 | Bicapped tetrahedron | C_s | 2.30 | 2.48 | 2.64 |
| Ni_4Pd_2 | Bicapped tetrahedron | C_{2v} | 2.32 | 2.47 | |
| Ni_5Pd_1 | Bicapped tetrahedron | C_s | 2.33 | 2.47 | |
| Ni_1Pd_6 | Capped octahedron | C_s | | 2.44 | 2.68 |
| Ni_2Pd_5 | Face-sharing trigonal bipyramid | C_1 | 2.30 | 2.50 | 2.66 |
| Ni_3Pd_4 | Capped octahedron | C_{3v} | 2.26 | 2.50 | 2.65 |
| Ni_4Pd_3 | Pentagonal bipyramid | C_{2v} | 2.32 | 2.51 | 2.75 |
| Ni_5Pd_2 | Pentagonal bipyramid | C_{2v} | 2.29 | 2.53 | |
| Ni_6Pd_1 | Capped octahedron | C_{3v} | 2.33 | 2.46 | |
| Ni_1Pd_7 | Dodecahedron | C_s | | 2.44 | 2.69 |
| Ni_2Pd_6 | Dodecahedron | C_s | | 2.47 | 2.73 |
| Ni_3Pd_5 | Fused octahedron with square pyramid | C_s | 2.28 | 2.48 | 2.63 |
| Ni_4Pd_4 | Dodecahedron | S_4 | 2.25 | 2.52 | 2.67 |
| Ni_5Pd_3 | Meta-bicapped octahedron | C_{2v} | 2.36 | 2.47 | |
| Ni_6Pd_2 | Meta-bicapped octahedron | C_{2v} | 2.35 | 2.46 | |
| Ni_7Pd_1 | Dodecahedron | C_s | 2.33 | 2.53 | |
| Ni_1Pd_8 | Face-sharing octahedra | C_{2v} | | 2.47 | 2.67 |
| Ni_2Pd_7 | Face-sharing octahedra | C_s | 2.31 | 2.49 | 2.67 |
| Ni_3Pd_6 | Face-sharing octahedra | D_{3h} | 2.29 | 2.51 | 2.66 |
| Ni_4Pd_5 | Two fused trigonal prisms capped on one square face | C_1 | 2.32 | 2.48 | 2.64 |
| Ni_5Pd_4 | Tricapped trigonal prism | C_1 | 2.32 | 2.48 | 2.87 |
| Ni_6Pd_3 | Tricapped trigonal prism | D_{3h} | 2.30 | 2.51 | |
| Ni_7Pd_2 | Tricapped trigonal prism | C_{2v} | 2.32 | 2.51 | |
| Ni_8Pd_1 | Tricapped trigonal prism | C_{2v} | 2.33 | 2.53 | |
| Ni_1Pd_9 | Incomplete centred icosahedron | C_{3v} | | 2.59 | 2.67 |
| Ni_2Pd_8 | Polytetrahedral structure | C_s | 2.35 | 2.48 | 2.66 |
| Ni_3Pd_7 | Polytetrahedral structure | C_s | 2.34 | 2.47 | 2.68 |
| Ni_4Pd_6 | Polytetrahedral structure | C_1 | 2.33 | 2.50 | 2.68 |
| Ni_5Pd_5 | Polytetrahedral structure | C_s | 2.31 | 2.52 | 2.64 |
| Ni_6Pd_4 | Tetracapped octahedron | T_d | 2.45 | 2.41 | |
| Ni_7Pd_3 | Tetracapped octahedron | C_{3v} | 2.39 | 2.41 | |
| Ni_8Pd_2 | Tetracapped octahedron | C_{2v} | 2.34 | 2.41 | |
| Ni_9Pd_1 | Tetracapped octahedron | C_{3v} | 2.38 | 2.42 | |

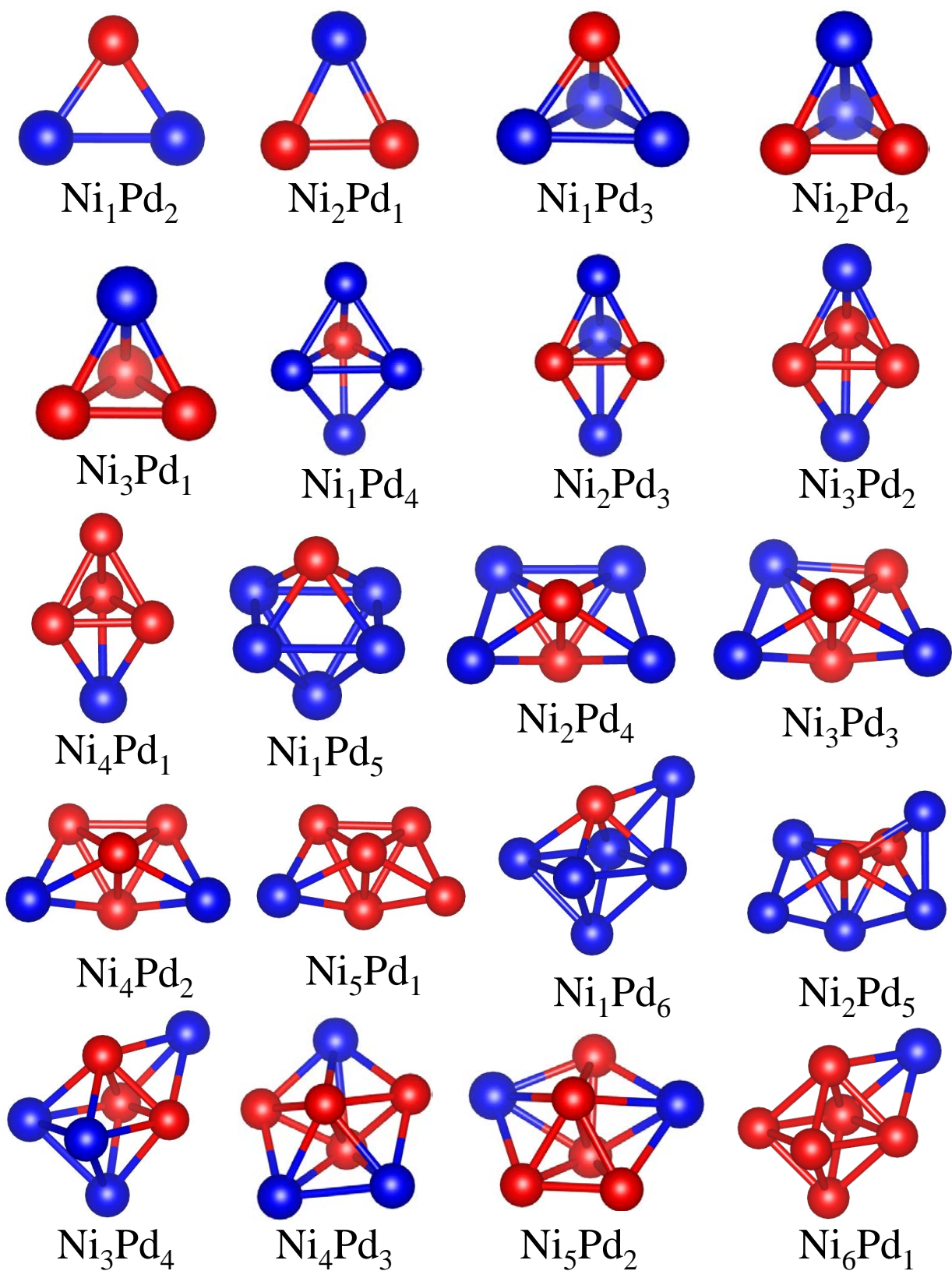


Figure 4: Putative global minimum structures for all compositions of Ni-Pd nanoalloys with sizes $N = 3 - 7$, Pd and Ni are shown (here, and in subsequent figures) in blue and red, respectively.

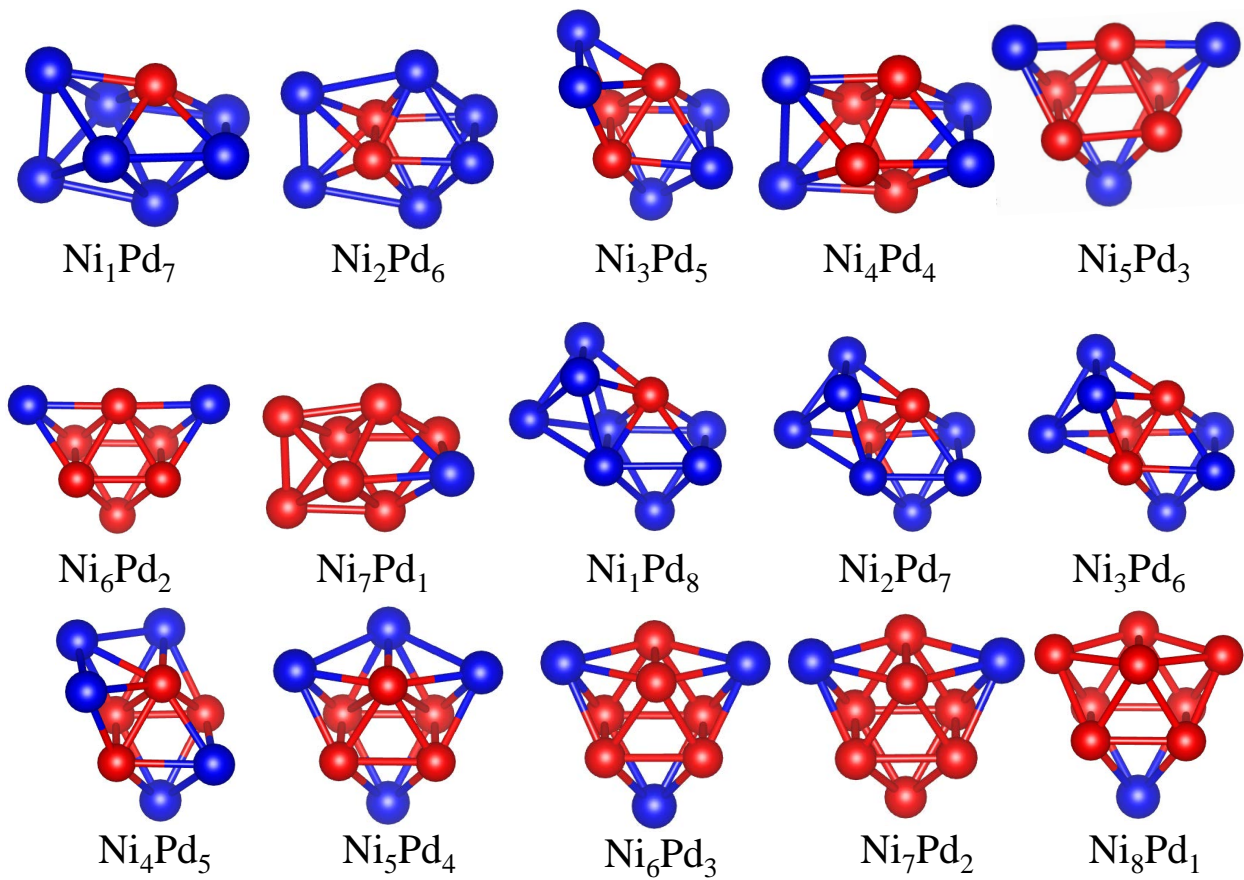


Figure 5: Putative global minimum structures for all compositions of Ni-Pd nanoalloys with sizes $N = 8 - 9$.

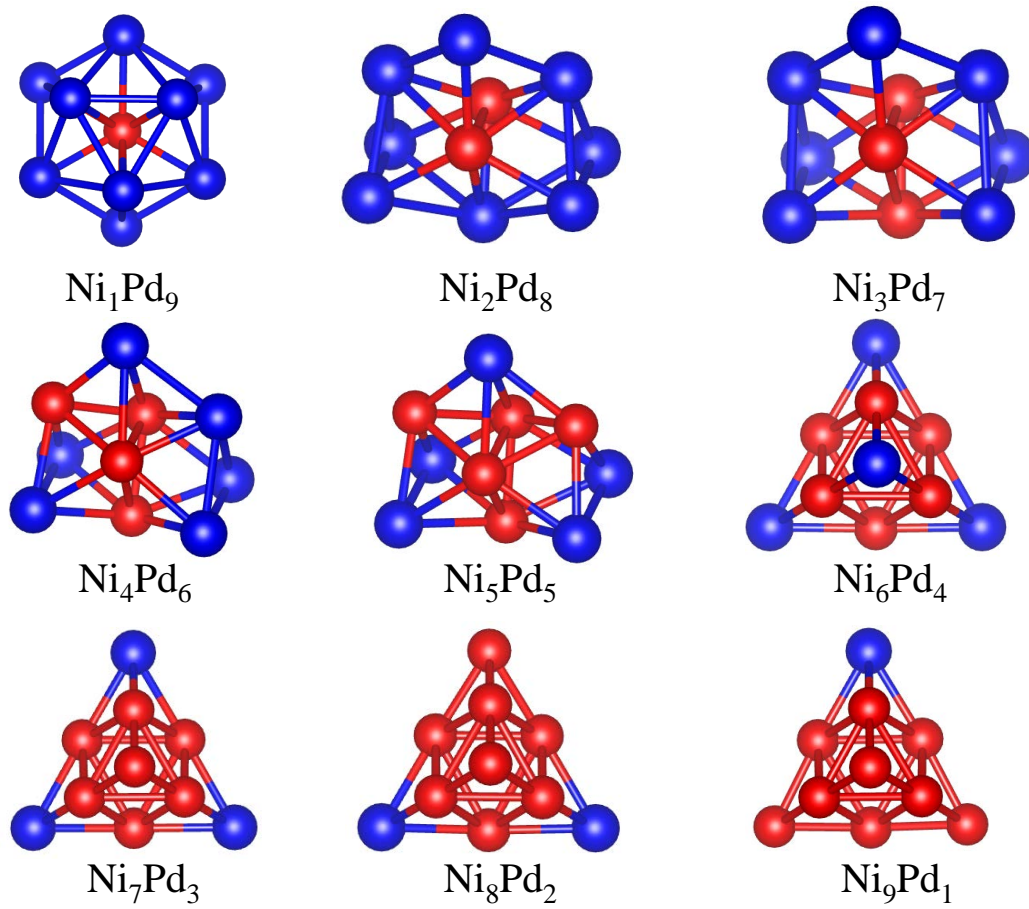


Figure 6: Putative global minimum structures for all compositions of Ni-Pd nanoalloys of size $N = 10$.

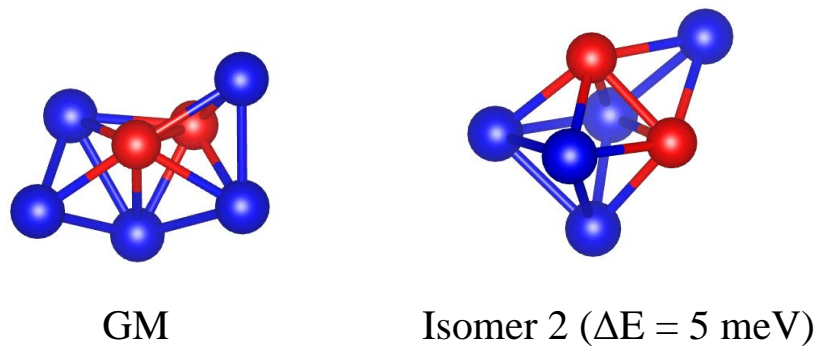


Figure 7: Quasi-degenerate Ni_2Pd_5 isomers.

Energetic analysis

To evaluate the stability of Ni-Pd clusters, we have to calculate the excess energy Δ , the second difference in energy $\Delta_2 E$, and the binding energy per atom E_b , which are defined in Eqs. (6), (7) and (8). These energies are listed in Tables S1 ($N = 3 - 8$ atoms) and S2 ($N = 9 - 10$ atoms).

Considering the bulk elemental properties of Ni and Pd (Table 6), such as surface energy (E_{surf}), cohesive energy (E_{coh}), atomic radius (r_a) and electronegativity (χ), we can predict the elemental segregation in Ni-Pd nanoalloys.

Table 6: Some elemental properties of Ni and Pd.³⁹

| | $E_{coh} / \text{eV atm}^{-1}$ | $E_{surf} / \text{meV } \text{\AA}^{-2}$ | $r_a / \text{\AA}$ | χ |
|----|--------------------------------|--|--------------------|--------|
| Pd | -3.89 | 131 | 1.38 | 2.2 |
| Ni | -4.44 | 149 | 1.25 | 1.8 |

The higher cohesive energy of Ni and the lower surface energy of Pd explains the tendency of Pd to segregate towards the surface in bulk Ni-Pd alloys.¹¹⁵⁻¹¹⁸ These properties together with the smaller atomic radius of Ni compared with Pd, favour the formation of Ni-Pd bimetallic clusters with Ni in the core and Pd on the shell. This Pd-segregation lowers the surface energy of the alloy.¹¹⁹ In addition, empirical and *ab initio* results agree that Ni-Pd hybridization enhances the magnetic moments of Ni atoms.³⁹

We have studied the effect of mixing in a cluster by calculating the excess energy (or mixing energy, Δ) as a function of the number of Ni atoms. Excess energy plots for Ni_mPd_n clusters with $4 \leq N \leq 10$ are shown in Figs. 8 and 9. Negative values of excess energies represent favourable mixing, whereas de-mixing is indicated by positive values of Δ .

All ($m + n = 3$), ($m + n = 4$) and ($m + n = 5$) clusters favour mixing and the strongest mixing (most negative Δ) are found for Ni_1Pd_2 , Ni_1Pd_3 and Ni_3Pd_2 , respectively. For ($m + n = 6$) clusters, Ni_5Pd_1 shows a strong de-mixing tendency, whereas Ni_2Pd_4 exhibits

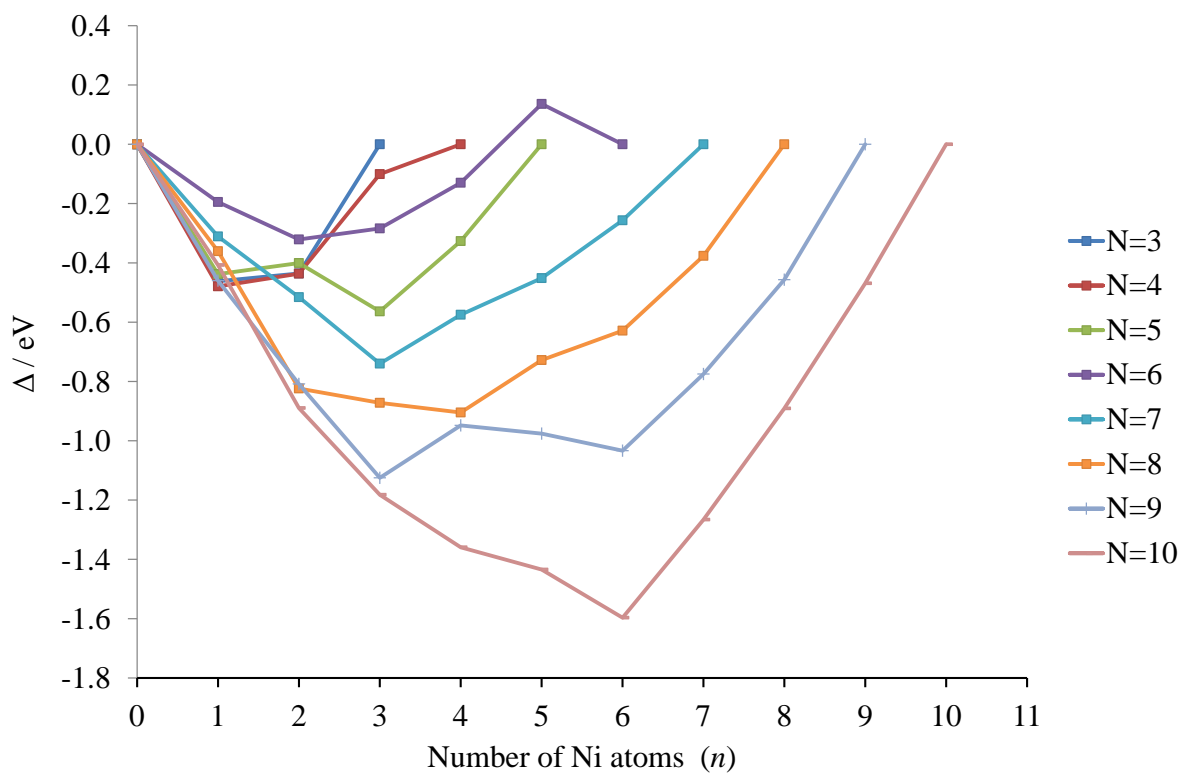


Figure 8: Plot of excess/mixing energy (Δ) against the number of Ni atoms (n) for Ni-Pd clusters with $N = 3 - 10$.

the best mixing. All of the other sizes, ($m + n = 7, 8, 9$ and 10) favour mixing, with the most favourable mixing being for Ni_3Pd_4 , Ni_4Pd_4 , Ni_3Pd_6 and Ni_6Pd_4 , respectively. In fact, we have found that the optimum values of Δ become more negative for larger clusters from around -0.4 eV for $N = 3 - 6$ to -1.6 eV for $N = 10$. This indicates that $N = 10$ has the strongest mixing tendency.

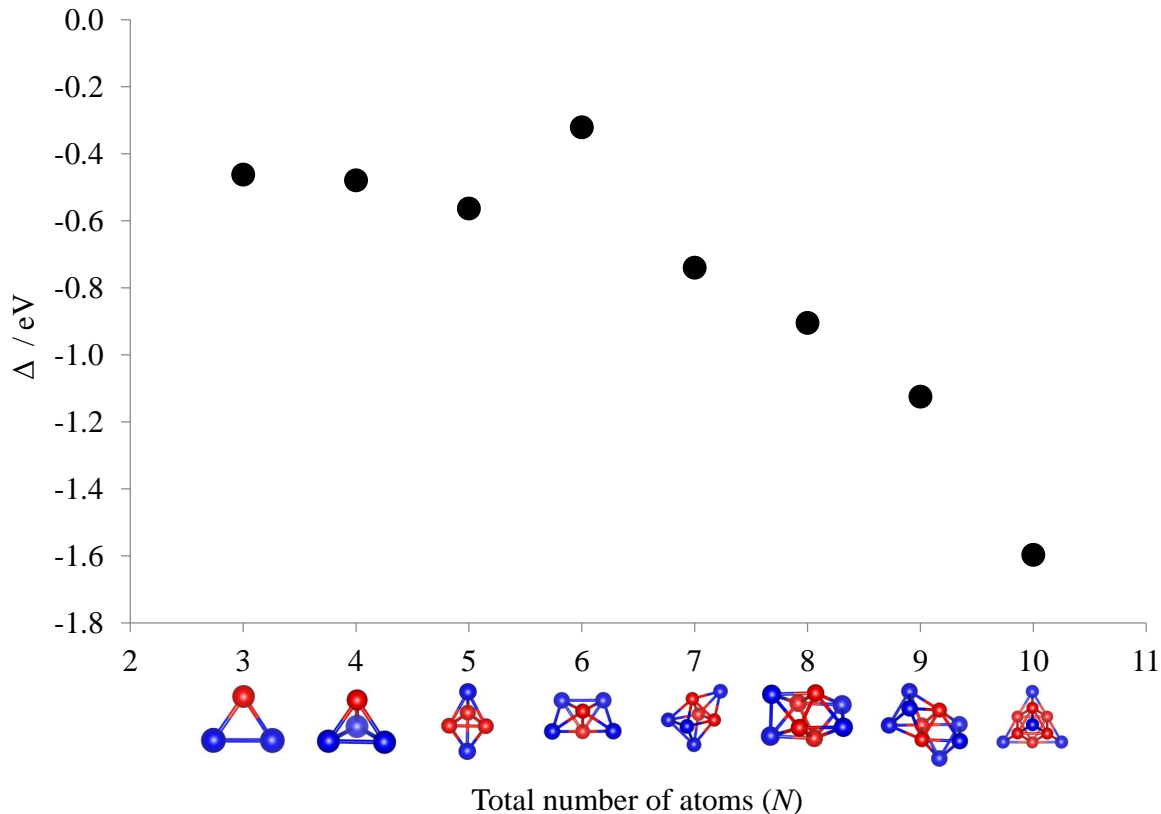


Figure 9: Ni-Pd isomers with lowest excess energies (Δ), indicating most favourable mixing, for $N = 3 - 10$ atoms.

The mixing energy values for clusters with the same size show that variations in composition plays a more important role than geometric effects in determining cluster stabilities.

The relative stabilities of pure Ni and Pd clusters with different nuclearities can be compared by calculating the second difference in energy $\Delta_2 E$, which indicates the stability of an N -atom cluster with respect to neighbouring sizes. Fig. 10 shows a plot of the second

difference in energy for Ni and Pd clusters as a function of cluster size. The most relatively stable clusters are indicated by significant positive peaks in Δ_2E .

Compared to their neighbours, Pd₄, Pd₆ and Pd₉ clusters exhibit high relative stability, while Pd₅, Pd₃, Pd₇ and Pd₈ are relatively unstable. The most stable cluster is Pd₄. The octahedral Ni₆ cluster is significantly more stable than its neighbours, suggesting it is "magic" size in the considered sub-nanometre regime.

For size $N = 6$, the findings show that free Ni₆ (3D) and Pd₆ (3D) clusters have a high relative stability compared to their neighbours. Accordingly, $N = 6$ represents a magic size for both 3D Ni and 3D Pd structures (in agreement with refs^{102,120,121} which already suggested that Pd₆ is a magic size or most stable Pd isomer). The magic size $N = 6$ for both free Ni and Pd clusters explains the positive or low negative values of mixing energy of nanoalloys compared to monometallic clusters at this size, as it is energetically difficult to induce the underlying mechanisms of mixing in binary metallic systems to leave their high stable composition to the less one, resulting high tendency of de-mixing at this size.

The stabilities of nanoclusters relative to their constituent ground state atoms is determined by calculating the binding energy per atom, E_b . A plot of the binding energies is shown in Fig. 11. According to the plot, the binding energy shows an increasing trend with cluster size. It can also be seen that the binding energy increases with increasing Ni composition (reflecting the stronger Ni-Ni and Ni-Pd bonds compared to Pd-Pd). For clusters of the same size, the binding energies decreases with the substitution of one Ni atom by one Pd atom. This is in agreement with the fact that the binding energies of Pd clusters are lower than those of the Ni clusters. Our calculations for the binding energy show good agreement with previous theoretical calculations.^{107,110}

Chemical stabilities of the clusters are investigated by analysing their HOMO-LUMO energy gaps (Δ_{HL}), with large Δ_{HL} indicating high stability of the system since Δ_{HL} indicates the ability of electron to hop from HOMO to LUMO. Figure 12 shows plots of Δ_{HL} as a function of the total number of atoms (N) for pure and mono-substituted clusters. Ni₄

(0.56 eV) has the highest Δ_{HL} among the pure and mono-substituted species studied in this work. Thus, one can expect high chemical stability for this cluster. Ni and Pd pure clusters are expected to have high chemical activity except for Ni_4 , Ni_{10} (0.30 eV) and Pd_2 (0.37 eV) which have large Δ_{HL} . However, mono-substituted clusters behave different from pure clusters. $\text{Ni}_{N-1}\text{Pd}_1$ plot shows marked odd-even alternations, with larger Δ_{HL} values for odd-atom clusters and smaller values for even-atom clusters. Doping a single Pd atom into the Ni clusters (Figure 12a) leads to an increase in Δ_{HL} for $N=3, 5, 7$ and 9 , while there is almost no difference for $N=6$ and 8 and a decrease in Δ_{HL} for $N=2, 4$ and 10 . When doping a single Ni atom into the Pd clusters (Figure 12b) leads to an increase in Δ_{HL} for $N=3-6$ and 9 , with the exception of $N=2$ and 8 where there is a considerable decrease. There is no significant difference for $N=7$ and 10 .

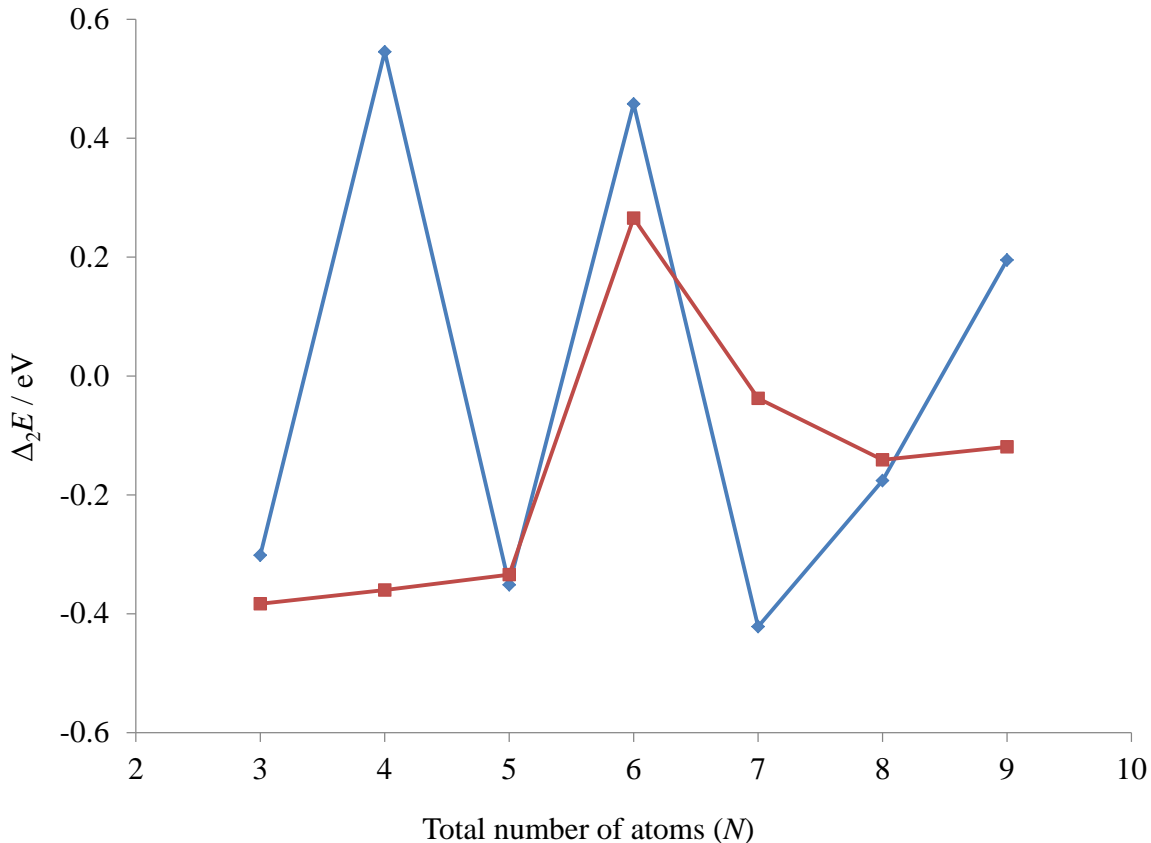


Figure 10: Second difference in energy $\Delta_2 E$ for pure Pd (blue) and Ni clusters (red).

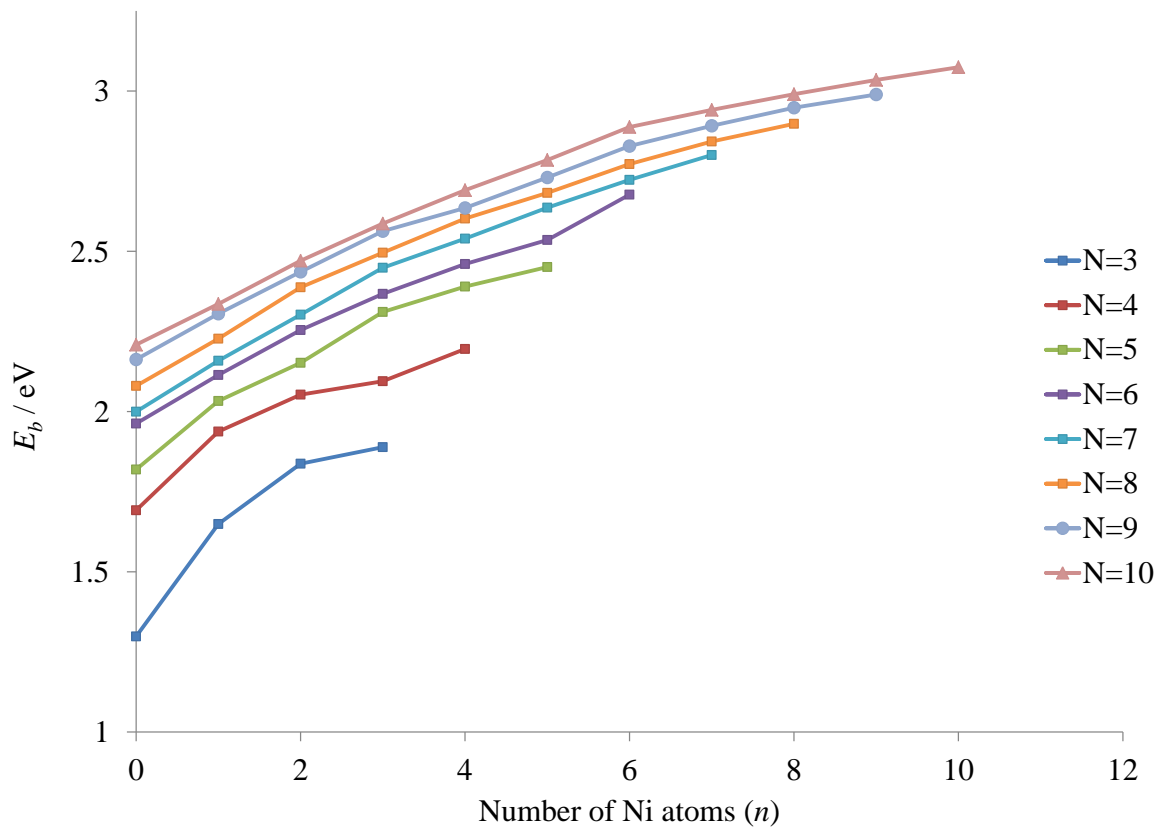


Figure 11: Plot of binding energies E_b of Ni_nPd_m clusters for sizes $N = 3 - 10$ against the number of Ni atoms (n).

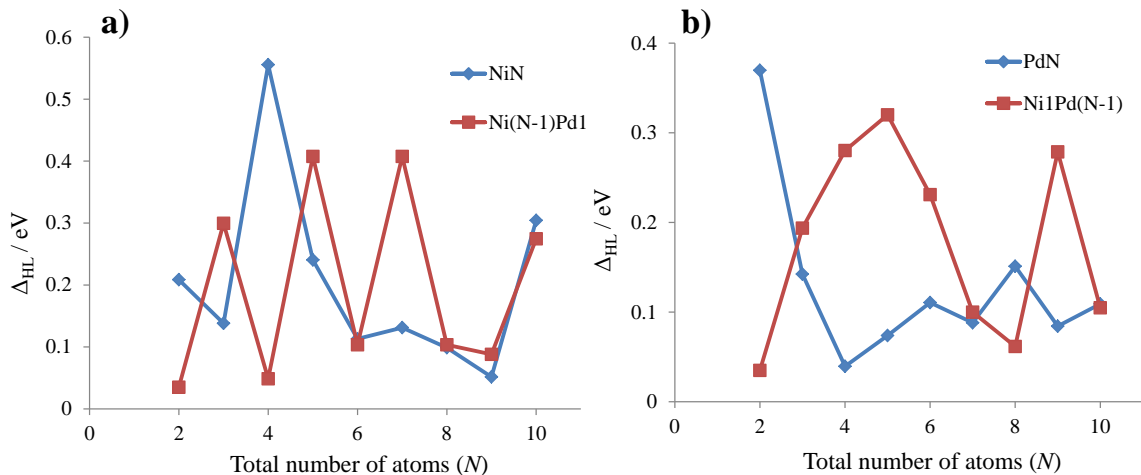


Figure 12: HOMO-LUMO energy gaps plotted against the total number of atoms, N , for free pure and mono-doped clusters ($N=2-10$).

As mentioned above, clusters with high HOMO-LUMO gaps are expected to show reduced reactivity. Hardness (η , Eqn. 4)¹²²⁻¹²⁶ is an important descriptor for the stability and reactivity of a given system and can be interpreted as the system's resistance to changing its electronic distribution of its electronegativity. It is well known that electrons should flow from lower electronegativity (χ) atoms to those of higher electronegativity (i.e. to lower the chemical potential). Our χ values (Eqn. 3) for most of the compositions reported in Figure 13 and Tables S3 and S4 in the Supporting Information, show that for $N=3, 4$ and 10 , Pd and Pd-rich clusters (with higher χ) hold their electrons more than Ni and Ni-rich clusters. For $N=5, 7$ and 9 , clusters with around 50:50 composition present higher χ than pure, Ni-rich and Pd-rich clusters. Systems with $N=6$ and 8 show several oscillations and Ni and Ni-rich clusters hold their electrons more than Pd and Pd-rich clusters.

Electrophilicity of a system is the measure of its reactivity towards attracting electrons from a nucleophile so that they form a bond. Our results show that in the majority of cases pure, Ni-rich and Pd-rich clusters present higher ω than clusters with around 50:50 composition (Tables S3 and S4).

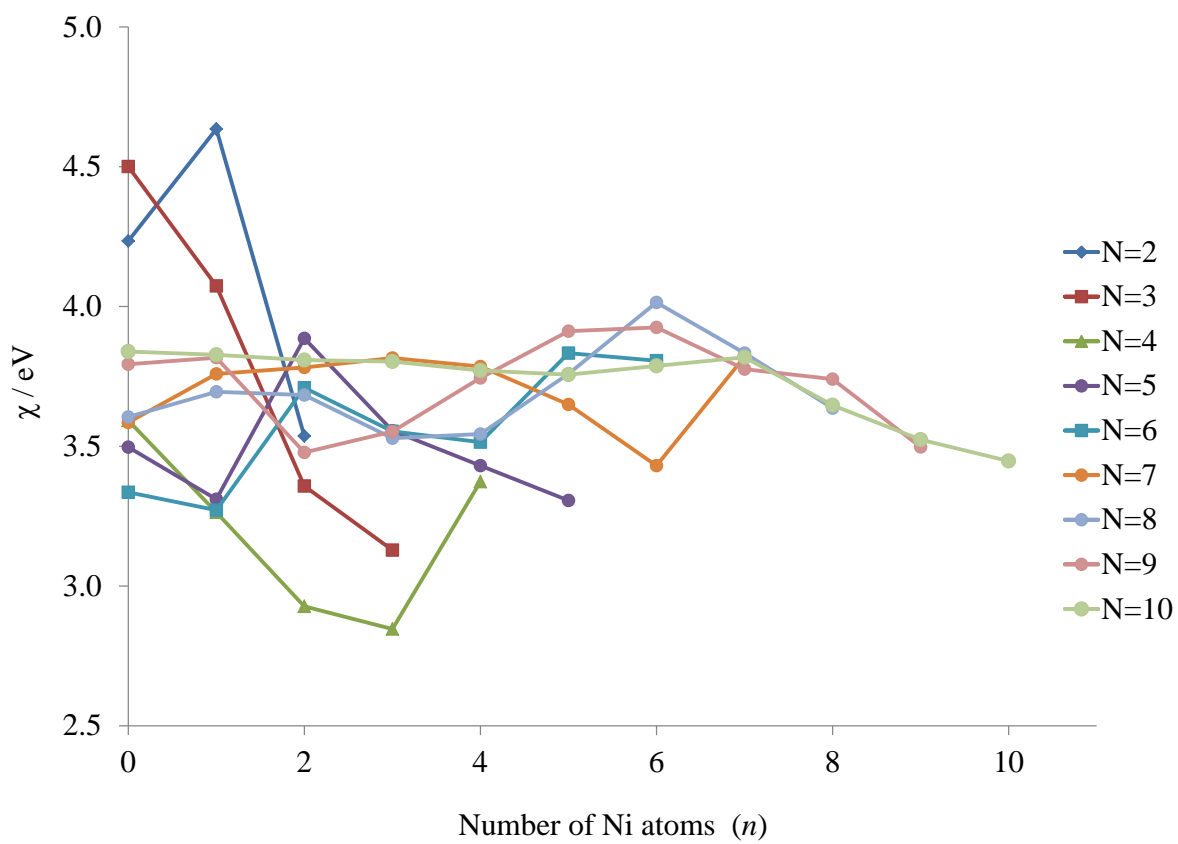


Figure 13: Electronegativity (χ) plotted against the number of Ni atoms, n .

Ni-Pd interactions can be strengthened by the Ni-Pd charge transfer. Bader charge analysis¹²⁷ (see Supporting Information, Tables S5-S12) shows that there is a 0.07 e⁻ charge transfer from Pd to Ni in the Ni-Pd dimer. For Ni-Pd clusters, the charge is found to be transferred from Ni to Pd. The calculated Ni-Pd charge transfers are between 0.23 and 0.41 e⁻ for Ni₁Pd_{*n*}, while for Ni_{*m*}Pd₁ clusters there is lower charge transfer (between 0.18 and 0.33 e⁻). The findings show when the composition get closer to 50:50 for Ni-Pd nanoalloys, the charge transfer decreases. This confirms that the suggested stability of the cluster isomers may also be enhanced by the charge transfers with Ni atoms occupying core positions, surrounded by Pd.

Systematic homotop search

The possible permutations of two different metals (Ni and Pd) in the system can be investigated by systematic homotop searches. The number of homotops grows exponentially with the size of the cluster.³⁹ The global minima of Ni-Pd nanoalloys have many symmetry inequivalent homotops which may have been missed by the MEGA-DFT search. Based on the global minima obtained clusters, we have studied the structural energy for symmetry inequivalent homotops of mono-substituted clusters by DFT local minimisation using the VASP code. Figs. 14 and 15 show plots of the relative energy $\Delta E(h_i)$ against symmetry inequivalent homotop structures for these clusters. The homotops are shown in Tables 7 and 8.

The MEGA-DFT search for all mono-substituted clusters $N = 5 - 10$, successfully found the lowest energy homotop as the global minimum. There are two important factors that determine the homotop stability. First, Pd atoms preferentially tend to occupy low-connectivity

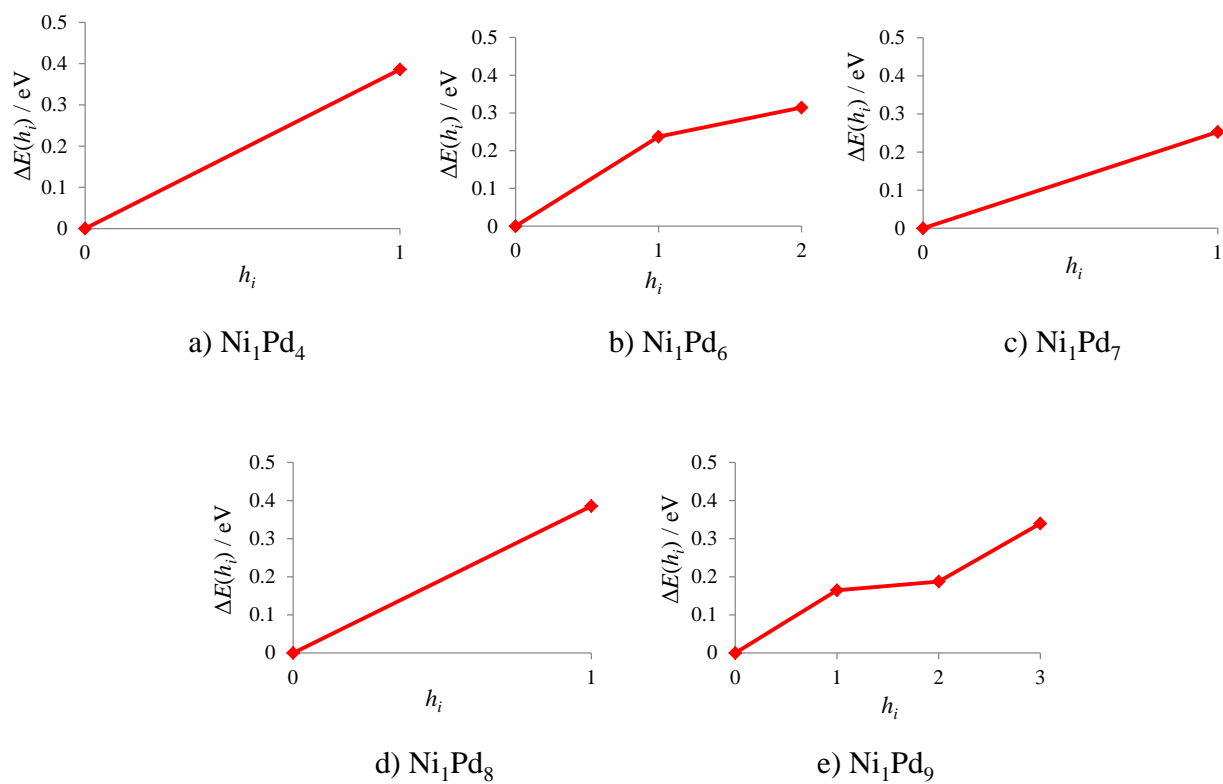


Figure 14: Relative energies of symmetry inequivalent homotops for several Ni₁-doped Pd clusters. Homotop 0 is the GM.

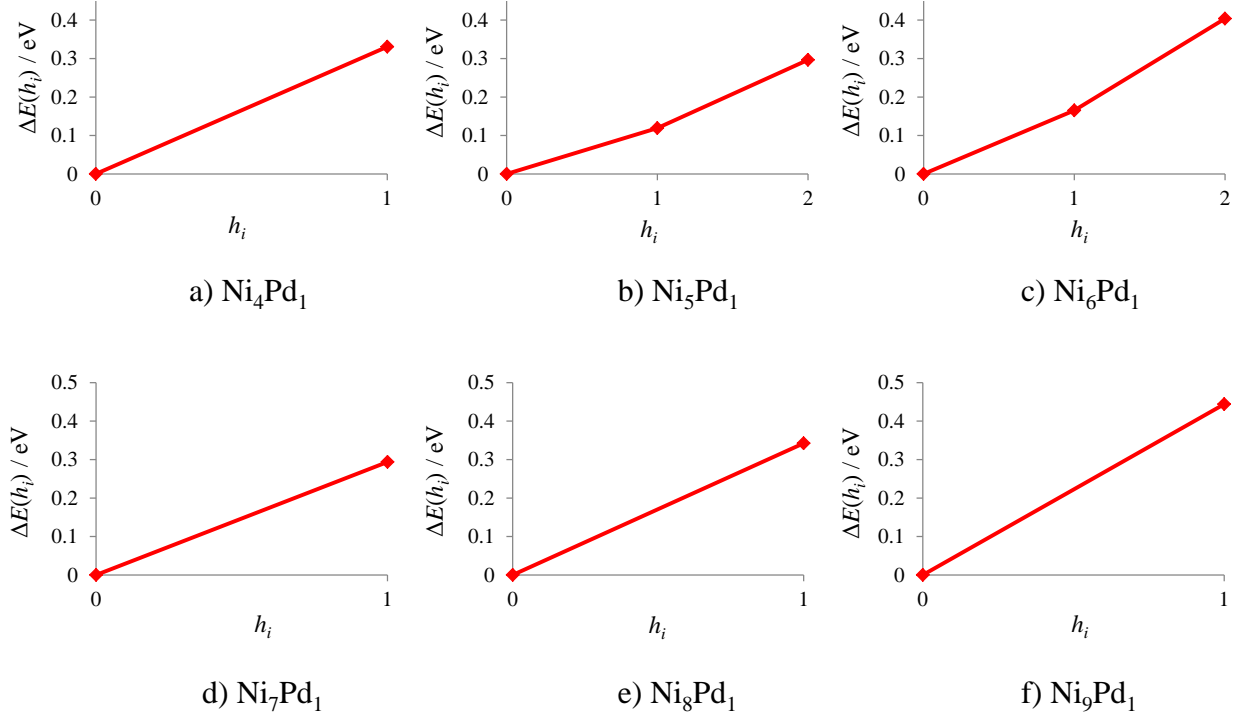


Figure 15: Relative energies of symmetry inequivalent homotops for several Pd_1 -doped Pd clusters. Homotop 0 is the GM.

sites, thereby maximizing the number of (stronger) Ni-Ni bonds. Second, Ni atoms tend to occupy high-connectivity sites, maximizing the number of Ni-Pd bonds, again correlating with bonds strengths and surface and cohesive energies (Table 6). For $N = 5$, Ni_1Pd_4 and Ni_4Pd_1 have one symmetry inequivalent homotop, with energies relative to the corresponding GM of 0.39 and 0.33 eV, respectively. The Ni atom in Ni_1Pd_4 forms four of the stronger Ni-Pd bonds in the GM, but there are only three Ni-Pd bonds in homotop (h_1). For Ni_4Pd_1 , the homotop with the Pd atom in the low-coordinate site maximises the number of the strongest Ni-Ni bonds (6).

For $N = 6$, Ni_1Pd_5 does not have any symmetry inequivalent homotops, whereas Ni_5Pd_1 has three symmetry inequivalent homotops which can clearly be seen in Fig. 15(b). The $\Delta E(h_i)$ are 0.12 eV (h_1) and 0.24 eV (h_2). Again, the Pd atom is found in the lowest connectivity site in the GM, while in the next homotop (h_1), the Pd atom is located in a different position forming another Ni-Pd bond, thereby decreasing the number of Ni-Ni

Table 7: Structures and energy differences for low energy homotops of free monosubstituted clusters, $N = m + n = 5 - 7$

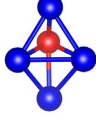
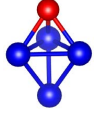
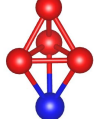
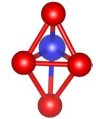
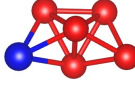
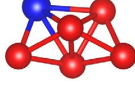
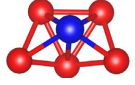
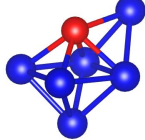
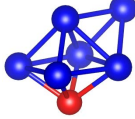

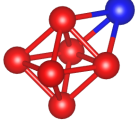
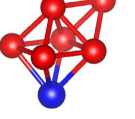
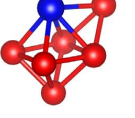
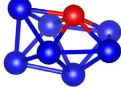
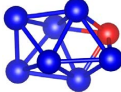
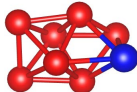
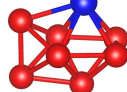
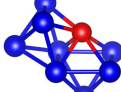
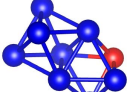
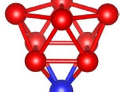
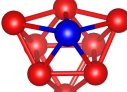
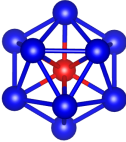
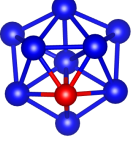
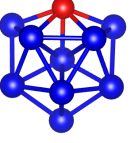
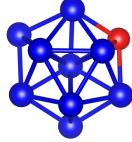
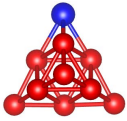
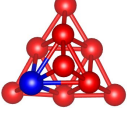
| N | Composition | GM (E/eV) | h_i (E/eV) |
|-----|---------------------------------|---|--|
| 5 | Ni ₁ Pd ₄ |  0.00 |  h_1 (0.39) |
| 5 | Ni ₄ Pd ₁ |  0.00 |  h_1 (0.33) |
| 6 | Ni ₅ Pd ₁ |  0.00 |  h_1 (0.12)  h_2 (0.30) |
| 7 | Ni ₁ Pd ₆ |  0.00 |  h_1 (0.24)  h_2 (0.31) |
| 7 | Ni ₆ Pd ₁ |  0.00 |  h_1 (0.17)  h_2 (0.40) |

Table 8: Structures and energy differences for low energy homotops of free monosubstituted clusters, $N = m + n = 8 - 10$

| N | Composition | GM (E/eV) | h_i (E/eV) |
|-----|---------------------------------|---|---|
| 8 | Ni ₁ Pd ₇ |  0.00 |  h_1 (0.25) |
| 8 | Ni ₇ Pd ₁ |  0.00 |  h_1 (0.29) |
| 9 | Ni ₁ Pd ₈ |  0.00 |  h_1 (0.39) |
| 9 | Ni ₈ Pd ₁ |  0.00 |  h_1 (0.34) |
| 10 | Ni ₁ Pd ₉ |  0.00 |  h_1 (0.16)  h_2 (0.19)  h_3 (0.34) |
| 10 | Ni ₉ Pd ₁ |  0.00 |  h_1 (0.44) |

bonds, and decreasing the homotop stability. Finally, in h_2 , the Pd atom is found in a position where it forms five Ni-Pd bonds, further the number of Ni-Ni bonds, and making h_2 less stable than h_1 . We have found the same behaviour for all the different mono-substituted nanoalloys (Ni_1Pd_n and Ni_mPd_1).

For $N = 7$, Ni_1Pd_6 and Ni_6Pd_1 both have two symmetry inequivalent homotops, which can clearly be seen in Fig. 14(b) and Fig. 15(c), respectively. $\Delta E(h_i)$ for Ni_1Pd_6 homotops are 0.24 eV (h_1) and 0.31 eV (h_2) and for Ni_6Pd_1 0.17 eV (h_1) and 0.40 eV (h_2).

For $N = 8$, Ni_1Pd_7 and Ni_7Pd_1 both have one symmetry inequivalent homotop, with relative energies (to the corresponding GM) of 0.25 and 0.29 eV, respectively. Fig. 14(d) and Fig. 15(e) show the relative energies for symmetry inequivalent homotops of Ni_1Pd_8 (0.39 eV) and Ni_8Pd_1 (0.34 eV). Finally, for $N = 10$, Ni_1Pd_9 has three inequivalent homotops which can clearly be seen in Fig. 14(e), with relative energies of 0.16 - 0.34 eV, whereas Ni_9Pd_1 has just one symmetry inequivalent homotop which is 0.44 eV less stable than the GM.

We have also studied the putative GM configuration and its inequivalent homotops for Ni_2Pd_3 (Fig. 16). The relative energies for the inequivalent homotops are 0.22 and 2.24 eV. The MEGA-DFT search successfully found the lowest energy homotop as GM of Ni_2Pd_3 cluster.

Conclusions

We have applied the DFT based-Mexican Enhanced Genetic Algorithm (MEGA-DFT) to Pd and Ni pure clusters and to Ni-Pd nanoalloys ranging from 3 to 10 atoms to investigate their properties. MEGA-DFT approach has successfully found the global minima. For single doped cluster, global minima structures were confirmed by homotop reminimisation. And,

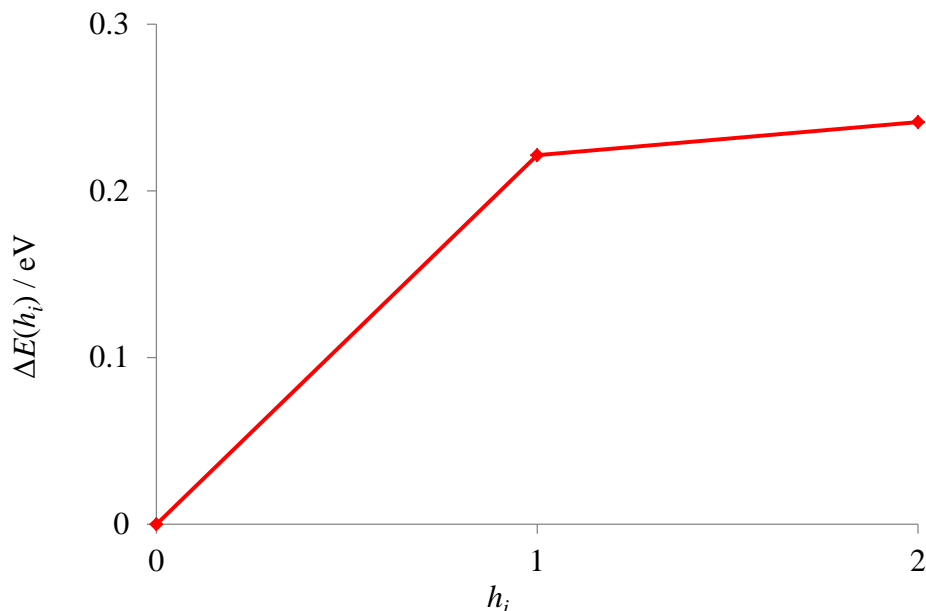


Figure 16: Relative energies of symmetry inequivalent homotops for for Ni_2Pd_3 . Homotop 0 is the GM.

a large number of spin configurations were considered to obtain the final lowest energy structures and magnetic moments.

All pure clusters (Ni or Pd) are 3D, but their structural motifs are found to be size-dependent. The structural behaviour for nanoalloys is controlled by the composition and size. Pd atoms tend to be located in low-connectivity surface sites, whereas Ni atoms generally prefer high-coordination positions in or close to the centre of the cluster. Spin magnetic moments for pure Ni clusters show oscillations for small sizes of the clusters.

A strong tendency of Ni-Pd clusters to alloy was predicted from calculated mixing energies. The second difference analysis indicates that Pd_4 , Pd_6 and Pd_9 clusters are more stable than their neighbours. The stabilities of cluster relative to their constituent increase with increasing cluster size are found to be higher for Ni and Ni-rich clusters.

Supporting Information

Supporting Information includes energies, spin magnetic moments (SMM), Excess Energies Δ , Binding Energies E_b , and the second difference in energy Δ_2E (Tables S1 and S2); HOMO-LUMO gap energies, ionization energies, electron affinities, electronegativity, global hardness and electrophilicity index (Tables S3 and S4). Bader charge (Tables S5-S12). This material is available free of charge via the Internet at <http://pubs.acs.org>.

Acknowledgments

This work was supported by Junta de Castilla y León and Fondo Social Europeo (Grant ORDEN EDU/310/2015, de 10 de abril and VA021G18) and MOVILIDAD DOCTORANDOS UVA 2017. Calculations were performed on the University of Birmingham's BlueBEAR high performance computer (<http://www.bear.bham.ac.uk/bluebear>). A. Granja-DelRío thanks Marc Jäger and John Hey for valuable help. A. Granja-DelRío also thanks Julio A. Alonso and María J. López for guiding her through the thesis period. Roy Johnston is pleased to dedicate this paper to Jean-François Halet (CNRS, Université de Rennes) on the occasion of his 60th birthday, with thanks for his friendship and in recognition of his valuable contributions to the computational study of organometallic molecules, clusters and solid state materials.

References

- (1) Fampiou, I.; Ramasubramaniam, A. Binding of Pt Nanoclusters to Point Defects in Graphene: Adsorption, Morphology, and Electronic Structure. *J. Phys. Chem. C* **2012**, *116*, 6543–6555.
- (2) Wang, H.; Robinson, J. T.; Diankov, G.; Dai, H. Nanocrystal Growth on Graphene with Various Degrees of Oxidation. *J. Am. Chem. Soc.* **2010**, *132*, 3270–3271.

- (3) Sun, Q.; Wang, Q.; Jena, P.; Kawazoe, Y. Clustering of Ti on a C₆₀ Surface and Its Effect on Hydrogen Storage. *J. Am. Chem. Soc.* **2005**, *127*, 14582–14583.
- (4) Freund, H. J. Metal Oxide Surfaces: Electronic Structure and Molecular Adsorption. *Phys. Status Solidi (b)* **1995**, *192*, 407–440.
- (5) Lee, S.; Fan, C.; Wu, T.; Anderson, S. L. CO Oxidation on Au_n/TiO₂ Catalysts Produced by Size-Selected Cluster Deposition. *J. Am. Chem. Soc.* **2004**, *126*, 5682–5683.
- (6) Qiao, B.; Wang, A.; Yang, X.; Allard, L.; Jiang, Z.; Cui, Y.; Liu, J.; Li, J.; Zhang, T. Single-Atom Catalysis of CO Oxidation Using Pt₁/FeO_x. *Nat. Chem.* **2011**, *3*, 634–641.
- (7) Chusuei, C. C.; Lai, X.; Luo, K.; Goodman, D. W. Modeling Heterogeneous Catalysts: Metal Clusters on Planar Oxide Supports. *Top. Catal.* **2000**, *14*, 71–83.
- (8) Kaden, W. E.; Wu, T.; Kunkel, W. A.; Anderson, S. L. Electronic Structure Controls Reactivity of Size-Selected Pd Clusters Adsorbed on TiO₂ Surfaces. *Science* **2009**, *326*, 826–829.
- (9) Kim, G.; Kawazoe, Y.; Lee, K.-R. Controlled Catalytic Properties of Platinum Clusters on Strained Graphene. *The J. Phys. Chem. Lett.* **2012**, *3*, 1989–1996.
- (10) Simon, P.; Gogotsi, Y. Materials for Electrochemical Capacitors. *Nat. Mater.* **2008**, *7*, 845–854.
- (11) Mahdy, A. M. E. DFT Study of Hydrogen Storage in Pd-Decorated C₆₀ Fullerene.
- (12) Satyapal, S.; Petrovic, J.; Thomas, G. Gassing up with Hydrogen. *Sci. Am.* **2007**, *296*, 80–87.
- (13) Dresselhaus, M. S.; Thomas, I. L. Alternative energy technologies. *Nature* **2001**, *414*, 332–337.

- (14) Cabria, I.; López, M. J.; Alonso, J. A. Theoretical Study of the Transition from Planar to Three-Dimensional Structures of Palladium Clusters Supported on Graphene. *Phys. Rev. B* **2010**, *81*, 035403.
- (15) Krasnov, P. O.; Ding, F.; Singh, A. K.; Yakobson, B. I. Clustering of Sc on SWNT and Reduction of Hydrogen Uptake: Ab-Initio All-Electron Calculations. *J. Phys. Chem. C* **2007**, *111*, 17977–17980.
- (16) Cabria, I.; López, M. J.; Fraile, S.; Alonso, J. A. Adsorption and Dissociation of Molecular Hydrogen on Palladium Clusters Supported on Graphene. *J. Phys. Chem. C* **2012**, *116*, 21179–21189.
- (17) López, M. J.; Cabria, I.; Alonso, J. A. Palladium Clusters Anchored on Graphene Vacancies and Their Effect on the Reversible Adsorption of Hydrogen. *J. Phys. Chem. C* **2014**, *118*, 5081–5090.
- (18) López-Corral, I.; Piriz, S.; Faccio, R.; Juan, A.; Avena, M. A Van der Waals DFT Study of PtH₂ Systems Absorbed on Pristine and Defective Graphene. *Appl. Surf. Sci.* **2016**, *382*, 80–87.
- (19) López-Corral, I.; de Celis, J.; Juan, A.; Irigoyen, B. DFT Study of H₂ Adsorption on Pd-Decorated Single Walled Carbon Nanotubes with C-Vacancies. *Int. J. Hydrogen Energy* **2012**, *37*, 10156–10164.
- (20) Yang, G. M.; Fan, X. F.; Shi, S.; Huang, H. H.; Zheng, W. Stability of Pt_n Cluster on Free/Defective Graphene: A First-Principles Study. *Appl. Surf. Sci.* **2017**, *392*, 936–941.
- (21) Heiz, U.; Sanchez, A.; Abbet, S.; Schneider, W.-D. Catalytic Oxidation of Carbon Monoxide on Monodispersed Platinum Clusters: Each Atom Counts. *J. Am. Chem. Soc.* **1999**, *121*, 3214–3217.

- (22) Schwank, J. Bimetallic Catalysts: Discoveries, Concepts, and Applications. *AIChE J.* **1985**, *31*, 1405–1405.
- (23) Teng, X.; Wang, Q.; Liu, P.; Han, W.; Frenkel, A. I.; Wen,; Marinkovic, N.; Hanson, J. C.; Rodriguez, J. A. Formation of Pd/Au Nanostructures from Pd Nanowires via Galvanic Replacement Reaction. *J. Am. Chem. Soc.* **2008**, *130*, 1093–1101.
- (24) Schön, G.; Simon, U. A Fascinating New Field in Colloid Science: Small Ligand-Stabilized Metal Clusters and Their Possible Application in Microelectronics. *Colloid Polym. Sci.* **1995**, *273*, 202–218.
- (25) Yang, F.; Deng, D.; Pan, X.; Fu, Q.; Bao, X. Understanding Nano Effects in Catalysis. *Natl. Sci. Rev.* **2015**, *2*, 183–201.
- (26) Wang, X.; Kariuki, N.; Niyogi, S.; Smith, M. C.; Myers, D. J.; Hofmann, T.; Zhang, Y.; Bär, M.; Heske, C. Bimetallic Palladium-Base Metal Nanoparticle Oxygen Reduction Electrocatalysts. *ECS Trans.* **2008**, *16*, 109–119.
- (27) Pachón, L. D.; Thathagar, M. B.; Hartl, F.; Rothenberg, G. Palladium-Coated Nickel Nanoclusters: New Hiyama Cross-Coupling Catalysts. *Phys. Chem. Chem. Phys.* **2006**, *8*, 151–157.
- (28) Levchenko, E. V.; Evteev, A. V.; Belova, I. V.; Murch, G. E. In *Defect and Diffusion Forum*, Proceedings of the Seventh International Conference on Diffusion in Materials, Lanzarote, Canary Islands, Spain, Oct 28-31, 2008; Agüero, A., Albella, J. M., Hierro, M. P., Philibert, J., Pérez Trujillo, F. J., Eds.; Trans Tech Publications Ltd, Switzerland, 2009.
- (29) Teranishi, T.; Miyake, M. Novel Synthesis of Monodispersed Pd/Ni Nanoparticles. *Chem. Mater.* **1999**, *11*, 3414–3416.

- (30) Son, S. U.; Jang, Y.; Park, J.; Na, H. B.; Park, H. M.; Yun, H. J.; Lee, J.; Hyeon, T. Designed Synthesis of Atom-Economical Pd/Ni Bimetallic Nanoparticle-Based Catalysts for Sonogashira Coupling Reactions. *J. Am. Chem. Soc.* **2004**, *126*, 5026–5027.
- (31) Ruban, A.; Hammer, B.; Stoltze, P.; Skriver, H. L.; rskov, J. K. N. Surface Electronic Structure and Reactivity of Transition and Noble Metals. *J. Mol. Catal. A: Chem.* **1997**, *115*, 421–429.
- (32) Mandal, M.; Kundu, S.; Ghosh, S.; Sau, T.; Yusuf, S.; Pal, T. Wet Chemical Method for Synthesis of Superparamagnetic Alloyed Ni-Pd and Ni-Pt Nanomagnets in Micelles. *J. Colloid Interface Sci.* **2003**, *265*, 23–28.
- (33) Lu, P.; Teranishi, T.; Asakura, K.; Miyake, M.; N.Toshima, Polymer-Protected Ni/Pd Bimetallic Nano-Clusters: Preparation, Characterization and Catalysis for Hydrogenation of Nitrobenzene. *J. Phys. Chem. B* **1999**, *103*, 9673–9682.
- (34) Reetz, M. T.; Helbig, W.; Quaiser, S. A. Electrochemical Preparation of Nanostructural Bimetallic Clusters. *Chem. Mater.* **1995**, *7*, 2227–2228.
- (35) Mörke, W.; Lamber, R.; Schubert, U.; Breitscheidel, B. Metal Complexes in Inorganic Matrixes. 11. Composition of Highly Dispersed Bimetallic Ni, Pd Alloy Particles Prepared by Sol-Gel Processing: Electron Microscopy and FMR Study. *Chem. Mater.* **1994**, *6*, 1659–1666.
- (36) Chang, C. M.; Chou, M. Y. Alternative Low-Symmetry Structure for 13-Atom Metal Clusters. *Phys. Rev. Lett.* **2004**, *93*, 133401.
- (37) Aguilera-Granja, F.; Longo, R. C.; Gallego, L. J.; Vega, A. Structural and Magnetic Properties of $X_{12}Y$ (X, Y=Fe, Co, Ni, Ru, Rh, Pd, and Pt) Nanoalloys. *J. Chem. Phys.* **2010**, *132*, 184507.

- (38) Heard, C. J.; Johnston, R. L. A Density Functional Global Optimisation Study of Neutral 8-Atom Cu-Ag and Cu-Au Clusters. *Eur. Phys. J. D* **2013**, *67*, 34.
- (39) Ferrando, R.; Jellinek, J.; Johnston, R. L. Nanoalloys: From Theory to Applications of Alloy Clusters and Nanoparticles. *Chem. Rev.* **2008**, *108*, 845–910.
- (40) Wales, D. J.; Doye, J. P. K. Global Optimization by Basin-Hopping and the Lowest Energy Structures of Lennard-Jones Clusters Containing up to 110 Atoms. *J. Phys. Chem. A* **1997**, *101*, 5111–5116.
- (41) Johnston, R. L. Evolving Better Nanoparticles: Genetic Algorithms for Optimising Cluster Geometries. *Dalton Trans.* **2003**, *22*, 4193–4207.
- (42) Wang, L.; Yamauchi, Y. Autoprogrammed Synthesis of Triple-Layered Au@Pd@Pt Core-Shell Nanoparticles Consisting of a Au@Pd Bimetallic Core and Nanoporous Pt Shell. *J. Am. Chem. Soc.* **2010**, *132*, 13636–13638.
- (43) Peng, Z.; Yang, H. Synthesis and Oxygen Reduction Electrocatalytic Property of Pt-on-Pd Bimetallic Heteronanostructures. *J. Am. Chem. Soc.* **2009**, *131*, 7542–7543.
- (44) Mazumder, V.; Sun, S. Oleylamine-Mediated Synthesis of Pd Nanoparticles for Catalytic Formic Acid Oxidation. *J. Am. Chem. Soc.* **2009**, *131*, 4588–4589.
- (45) Antolini, E. Palladium in Fuel Cell Catalysis. *Energy Environ. Sci.* **2009**, *2*, 915–931.
- (46) Shao, M. Palladium-Based Electrocatalysts for Hydrogen Oxidation and Oxygen Reduction Reactions. *J. Power Sources* **2011**, *196*, 2433–2444.
- (47) Pelzer, A. W.; Jellinek, J.; Jackson, K. A. H₂ Saturation on Palladium Clusters. *J. Phys. Chem. A* **2015**, *119*, 3594–3603.
- (48) Granja-DelRío, A.; Alonso, J. A.; López, M. J. Steric and Chemical Effects on the Hydrogen Adsorption and Dissociation on Free and Graphene-Supported Palladium Clusters. *Comput. Theor. Chem.* **2017**, *1107*, 23–29.

- (49) Xiao, L.; Wang, L. Structures of Platinum Clusters: Planar or Spherical? *J. Phys. Chem. A* **2004**, *108*, 8605–8614.
- (50) Toshima, N.; Yonezawa, T.; Kushihashi, K. Polymer-Protected Palladium-Platinum Bimetallic Clusters: Preparation, Catalytic Properties and Structural Considerations. *J. Chem. Soc., Faraday Trans.* **1993**, *89*, 2537–2543.
- (51) Zhang, K.; Xiang, Y.; Wu, X.; Feng, L.; He, W.; Liu, J.; Zhou, W.; Xie, S. Enhanced Optical Responses of Au@Pd Core/Shell Nanobars. *Langmuir* **2009**, *25*, 1162–1168.
- (52) Mu, Y.; Han, Y.; Wang, J.; Wan, J.; Wang, G. Structures and Magnetic Properties of Pd_n Clusters ($n = 3-19$) Doped by Mn Atoms. *Phys. Rev. A* **2011**, *84*, 053201.
- (53) Granja-DelRío, A.; Alonso, J. A.; López, M. J. Competition Between Palladium Clusters and Hydrogen to Saturate Graphene Vacancies. *J. Phys. Chem. C* **2017**, *121*, 10843–10850.
- (54) Davis, J. B. A.; Horswell, S. L.; Johnston, R. L. Global Optimization of 8-10 Atom Palladium-Iridium Nanoalloys at the DFT Level. *J. Phys. Chem. A* **2014**, *118*, 208–214.
- (55) Tan, J. L.; Jesus, A. M. D.; Chua, S. L.; Sanetuntikul, J.; Shanmugam, S.; Tongol, B. J. V.; Kim, H. Preparation and Characterization of Palladium-Nickel on Graphene Oxide Support as Anode Catalyst for Alkaline Direct Ethanol Fuel Cell. *Appl. Catal., A* **2017**, *531*, 29–35.
- (56) Calderón, J. C.; Celorrio, V.; Nieto-Monge, M. J.; Fermín, D. J.; Pardo, J. I.; Moliner, R.; Lázaro, M. Palladium-Nickel Materials as Cathode Electrocatalysts for Alkaline Fuel Cells. *Int. J. Hydrogen Energy* **2016**, *41*, 22538–22546.
- (57) Nieves-Torres, S.; Mo, E.; López, G. E. Bimetallic Ni/Pd Finite Systems: Structure

- and Thermodynamics of Bimetallic Ni/Pd Nanostructures in Two and Three Dimensions. *Mater. Chem. Phys.* **2011**, *129*, 580–585.
- (58) Filhol, J.-S.; Simon, D.; Sautet, P. Surface Phase Stability Diagram for Pd Deposits on Ni(110): A First-Principles Theoretical Study. *Phys. Rev. B* **2001**, *64*, 085412.
- (59) Filhol, J.-S.; Simon, D.; Sautet, P. Understanding the High Activity of a Nanostructured Catalyst Obtained by a Deposit of Pd on Ni: First Principle Calculations. *J. Am. Chem. Soc.* **2004**, *126*, 3228–3233.
- (60) Hermannsdörfer, J.; Friedrich, M.; Miyajima, N.; Albuquerque, R. Q.; Kümmel, S.; Kempe, R. Ni/Pd@MIL-101: Synergistic Catalysis with Cavity-Conform Ni/Pd Nanoparticles. *Angew. Chem., Int. Ed.* **2012**, *51*, 11473–11477.
- (61) Seif, A.; López, M. J.; Granja-DelRío, A.; Azizi, K.; Alonso, J. Adsorption and Growth of Palladium Clusters on Graphdiyne. *Phys. Chem. Chem. Phys.* **2017**, *19*, 19094–19102.
- (62) Gao, W.; Mueller, J. E.; Anton, J.; Jiang, Q.; Jacob, T. Nickel Cluster Growth on Defect Sites of Graphene: A Computational Study. *Angew. Chem., Int. Ed.* **2013**, *52*, 14237–14241.
- (63) Bouarab, S.; Vega, A.; López, M.; Iñíguez, M. P.; Alonso, J. A. Geometrical Effects on the Magnetism of Small Ni Clusters. *Phys. Rev. B* **1997**, *55*, 13279–13282.
- (64) Granja, A.; Alonso, J. A.; Cabria, I.; López, M. J. Competition Between Molecular and Dissociative Adsorption of Hydrogen on Palladium Clusters Deposited on Defective Graphene. *RSC Adv.* **2015**, *5*, 47945–47953.
- (65) Zhou, C.; Yao, S.; Wu, J.; Forrey, R. C.; Chen, L.; Tachibana, A.; Cheng, H. Hydrogen Dissociative Chemisorption and Desorption on Saturated Subnano Palladium Clusters (Pd_n, n=2-9). *Phys. Chem. Chem. Phys.* **2008**, *10*, 5445–5451.

- (66) Pelzer, A. W.; Jellinek, J.; Jackson, K. A. H₂ Reactions on Palladium Clusters. *J. Phys. Chem. A* **2013**, *117*, 10407–10415.
- (67) Liu, X.; Tian, D.; Meng, C. DFT Study on the Adsorption and Dissociation of H₂ on Pd_n (n=4, 6, 13, 19, 55) Clusters. *J. Mol. Struct.* **2015**, *1080*, 105–110.
- (68) Davis, J. B. A.; Shayeghi, A.; Horswell, S. L.; Johnston, R. L. The Birmingham Parallel Genetic Algorithm and its Application to the Direct DFT Global Optimisation of Ir_N (N = 10-20) Clusters. *Nanoscale* **2015**, *7*, 14032–14038.
- (69) Buendía, F.; Vargas, J. A.; Beltrán, M. R.; Davis, J. B. A.; Johnston, R. L. A Comparative Study of Au_mRh_n (4 ≤ m + n ≤ 6) Clusters in the Gas Phase Versus Those Deposited on (100) MgO. *Phys. Chem. Chem. Phys.* **2016**, *18*, 22122–22128.
- (70) Demiroglu, I.; Yao, K.; Hussein, H. A.; Johnston, R. L. DFT Global Optimization of Gas-Phase Subnanometer Ru-Pt Clusters. *J. Phys. Chem. C* **2017**, *121*, 10773–10780.
- (71) Davis, J. B. A.; Horswell, S. L.; Johnston, R. L. Application of a Parallel Genetic Algorithm to the Global Optimization of Gas-Phase and Supported Gold-Iridium Sub-Nanoalloys. *J. Phys. Chem. C* **2016**, *120*, 3759–3765.
- (72) Vargas, J. A.; Buendía, F.; Beltrán, M. R. New Au_N (N = 27-30) Lowest Energy Clusters Obtained by Means of an Improved DFT-Genetic Algorithm Methodology. *J. Phys. Chem. C* **2017**, *121*, 10982–10991.
- (73) Nayak, S. K.; Khanna, S. N.; Rao, B. K.; Jena, P. Physics of Nickel Clusters: Energetics and Equilibrium Geometries. *J. Phys. Chem. A* **1997**, *101*, 1072–1080.
- (74) Reddy, B. V.; Nayak, S. K.; Khanna, S. N.; Rao, B. K.; Jena, P. Physics of Nickel Clusters. 2. Electronic Structure and Magnetic Properties. *J. Phys. Chem. A* **1998**, *102*, 1748–1759.

- (75) Goel, S.; Masunov, A. E. Density Functional Theory Study of Small Nickel Clusters. *J. Mol. Model.* **2012**, *18*, 783–790.
- (76) Derosa, P. A.; Seminario, J. M.; Balbuena, P. B. Properties of Small Bimetallic Ni-Cu Clusters. *J. Phys. Chem. A* **2001**, *105*, 7917–7925.
- (77) Harb, M.; Rabilloud, F.; Simon, D. Density Functional Study of Structural and Electronic Properties of Small Bimetallic Silver-Nickel Clusters. *J. Phys. Chem. A* **2007**, *111*, 7726–7731.
- (78) Singh, P. P. Relativity and Magnetism in Ni-Pd and Ni-Pt Alloys. *J. Magn. Magn. Mater.* **2003**, *261*, 347–352.
- (79) Akai, H. Electronic Structure Ni-Pd Alloys Calculated by the Self-Consistent KKR-CPA Method. *J. Phys. Soc. Jpn.* **1982**, *51*, 468–474.
- (80) Buendía, F.; Vargas, J. A.; Johnston, R. L.; Beltrán, M. R. Study of the Stability of Small AuRh Clusters Found by a Genetic Algorithm Methodology. *Comput. Theor. Chem.* **2017**, *1119*, 51–58.
- (81) Kresse, G.; Hafner, J. Ab Initio Molecular Dynamics for Liquid Metals. *Phys. Rev. B* **1993**, *47*, 558–561.
- (82) Kresse, G.; Hafner, J. Ab Initio Molecular-Dynamics Simulation of the Liquid-Metal-Amorphous-Semiconductor Transition in Germanium. *Phys. Rev. B* **1994**, *49*, 14251–14269.
- (83) Kresse, G.; Furthmüller, J. Efficiency of Ab-Initio Total Energy Calculations for Metals and Semiconductors Using a Plane-Wave Basis Set. *Comput. Mater. Sci.* **1996**, *6*, 15–50.
- (84) Kresse, G.; Furthmüller, J. Efficient Iterative Schemes for Ab Initio Total-Energy Calculations Using a Plane-Wave Basis Set. *Phys. Rev. B* **1996**, *54*, 11169–11186.

- (85) Shayeghi, A.; Götz, D.; Davis, J. B.; Schäfer, R.; Johnston, R. L. Pool-BCGA: a Parallelised Generation-Free Genetic Algorithm for the Ab Initio Global Optimisation of Nanoalloy Clusters. *Phys. Chem. Chem. Phys.* **2015**, *17*, 2104–2112.
- (86) Deaven, D. M.; Ho, K. M. Molecular Geometry Optimization with a Genetic Algorithm. *Phys. Rev. Lett.* **1995**, *75*, 288–291.
- (87) Perdew, J. P.; Burke, K.; Ernzerhof, M. Generalized Gradient Approximation Made Simple. *Phys. Rev. Lett.* **1996**, *77*, 3865–3868.
- (88) Kresse, G.; Joubert, D. From Ultrasoft Pseudopotentials to the Projector Augmented-Wave Method. *Phys. Rev. B* **1999**, *59*, 1758–1775.
- (89) Frisch, M. J.; Trucks, G. W.; Schlegel, H. B.; Scuseria, G. E.; Robb, M. A.; Cheeseman, J. R.; Scalmani, G.; Barone, V.; Mennucci, B.; Petersson, G. A. et al. GAUSSIAN 09, Revision E.01, Gaussian Inc., Wallingford, CT, 2009.
- (90) Chai, J. D.; Head-Gordon, M. Long-Range Corrected Hybrid Density Functionals with Damped Atom-Atom Dispersion Corrections. *Phys. Chem. Chem. Phys.* **2008**, *10*, 6615–6620.
- (91) Chai, J. D.; Head-Gordon, M. Systematic Optimization of Long-Range Corrected Hybrid Density Functionals. *J. Chem. Phys.* **2008**, *128*, 084106.
- (92) Weigend, F.; Ahlrichs, R. Balanced Basis Sets of Split Valence, Triple Zeta Valence and Quadruple Zeta Valence Quality for H to Rn: Design and Assessment of Accuracy. *Phys. Chem. Chem. Phys.* **2005**, *7*, 3297–3305.
- (93) Weigend, F. Accurate Coulomb-Fitting Basis Sets for H to Rn. *Phys. Chem. Chem. Phys.* **2006**, *8*, 1057–1065.
- (94) Raju, R. K.; Rodriguez, P.; Johnston, R. L. Can a Single Valence Electron Alter

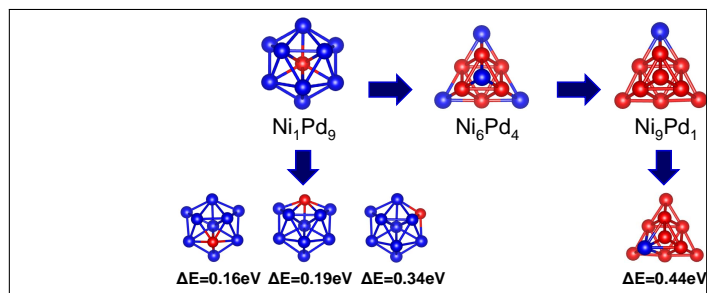
- the Electrocatalytic Activity and Selectivity for CO₂ Reduction on the Subnanometer Scale? *J. Phys. Chem. C* **2019**, *123*, 14591–14609.
- (95) Koopmans, T. Über die Zuordnung von Wellenfunktionen und Eigenwerten zu den Einzelnen Elektronen Eines Atoms. *Physica* **1934**, *1*, 104–113.
- (96) Jellinek, J.; Krissinel, E. B. Ni_nAl_m Alloy Clusters: Analysis of Structural Forms and Their Energy Ordering. *Chem. Phys. Lett.* **1996**, *258*, 283–292.
- (97) Huber, K.; Herzberg, G. *Molecular Structure and Molecular Spectra IV. Constants of Diatomic Molecules*; Springer US: New York, U. S. A, 1979.
- (98) Morse, M. D. Clusters of Transition-Metal Atoms. *Chem. Rev.* **1986**, *86*, 1049–1109.
- (99) Onal, I.; Sayar, A.; Uzun, A.; Ozkar, S. A Density Functional Study of Ni₂ and Ni₁₃ Nanoclusters. *J. Comput. Theor. Nanosci.* **2009**, *6*, 867–872.
- (100) Chen, B.; Castleman, A. W.; Ashman, C.; Khanna, S. N. NH₃ Adsorption Around Ni_n (n ≤ 4) Clusters. *Int. J. Mass Spectrom.* **2002**, *220*, 171 – 182.
- (101) Castro, M.; Jamorski, C.; Salahub, D. R. Structure, Bonding, and Magnetism of Small Fe_n, Co_n, and Ni_n Clusters, n ≤ 5. *Chem. Phys. Lett.* **1997**, *271*, 133 – 142.
- (102) Hussein, H. A.; Davis, J. B. A.; Johnston, R. L. DFT Global Optimisation of Gas-Phase and MgO-Supported Sub-Nanometre AuPd Clusters. *Phys. Chem. Chem. Phys.* **2016**, *18*, 26133–26143.
- (103) Zanti, G.; Peeters, D. DFT Study of Bimetallic Palladium-Gold Clusters Pd_nAu_m of Low Nuclearities (n + m ≤ 14). *J. Phys. Chem. A* **2010**, *114*, 10345–10356.
- (104) Moseler, M.; Häkkinen, H.; Barnett, R. N.; Landman, U. Structure and Magnetism of Neutral and Anionic Palladium Clusters. *Phys. Rev. Lett.* **2001**, *86*, 2545–2548.

- (105) Aguilera-Granja, F.; Vega, A.; Rogan, J.; García, G. Metallic Behavior of Pd Atomic Clusters. *Nanotechnology* **2007**, *18*, 365706.
- (106) Hernández-Torres, J.; Aguilera-Granja, F.; Vega, A. In *Physics of Low Dimensional Systems*, 1st ed.; Morán-López, J. L., Ed.; Springer: Boston, MA, 2001; pp 77–85.
- (107) Sahoo, S.; Rollmann, G.; Entel, P. First-Principles Calculation of Cluster Geometries and Magnetization of Pure Ni and Fe-Ni Clusters. *Phase Transitions* **2005**, *78*, 723–731.
- (108) Aguilera-Granja, F.; Longo, R. C.; Gallego, L. J.; Vega, A. Magnetic Cooperative Effects in Small Ni-Ru Clusters. *J. Phys. Chem. A* **2011**, *115*, 13950–13955.
- (109) Xie, Z.; Ma, Q.-M.; Liu, Y.; Li, Y.-C. First-Principles Study of the Stability and Jahn-Teller Distortion of Nickel Cluster. *Phys. Lett. A* **2005**, *342*, 459–467.
- (110) Aguilera-Granja, F.; Bouarab., S.; López, M. J.; Vega, A.; Montejano-Carrizales, J. M.; Iñíguez, M. P.; Alonso, J. A. Magnetic Moments of Ni Clusters. *Phys. Rev. B* **1998**, *57*, 12469–12475.
- (111) Wang, B.; Han, H.; Xie, Z. Structural and Magnetic Properties of Small Ni_nMn Clusters. *J. Mol. Struct.* **2014**, *1062*, 174–178.
- (112) Billas, I. M.; Châtelain, A.; de Heer, W. A. Magnetism from the Atom to the Bulk in Iron, Cobalt, and Nickel Clusters. *Science* **1994**, *265*, 1682–1684.
- (113) Billas, I. M.; Châtelain, A.; de Heer, W. A. Magnetic Moments of Iron Clusters with 25 to 700 Atoms and their Dependence on Temperature. *Phys. Rev. Lett.* **1993**, *71*, 4067–4070.
- (114) Liu, F.; Press, M. R.; Khanna, S. N.; Jena, P. Magnetism and Local Order: Ab Initio Tight-Binding Theory. *Phys. Rev. B* **1989**, *39*, 6914–6924.

- (115) Yu, Y.; Xiao, W.; Wang, J.; Wang, L. Understanding the Surface Segregation Behavior of Transition Metals on Ni(111): a First-Principles Study. *Phys. Chem. Chem. Phys.* **2016**, *18*, 26616–26622.
- (116) Bozzolo, G.; Noebe, R. D. Analysis of Surface and Bulk Behavior in Ni-Pd Alloys. *Acta Mater.* **2003**, *51*, 4395–4409.
- (117) Ruban, A. V.; Skriver, H. L.; Nørskov, J. K. Surface Segregation Energies in Transition-Metal Alloys. *Phys. Rev. B* **1999**, *59*, 15990–16000.
- (118) Cui, M.; Liu, H.; Jiang, H.; Cao, Z.; Meng, X. Phase Diagram of Continuous Binary Nanoalloys: Size, Shape, and Segregation Effects. *Sci. Rep.* **2017**, *7*, 41990.
- (119) Helfensteyn, S.; Luyten, J.; Feyaerts, L.; Creemers, C. Modelling Surface Phenomena in Pd-Ni Alloys. *Appl. Surf. Sci.* **2003**, *212-213*, 844–849.
- (120) Gao, X.; Chen, W. Highly Stable and Efficient Pd₆(SR)₁₂ Cluster Catalysts for the Hydrogen and Oxygen Evolution Reactions. *Chem. Commun.* **2017**, *53*, 9733–9736.
- (121) Kwon, G.; Ferguson, G. A.; Heard, C. J.; Tyo, E. C.; Yin, C.; DeBartolo, J.; Seifert, S.; Winans, R. E.; Kropf, J. A.; Greeley, J. et al. Size-Dependent Subnanometer Pd Cluster (Pd₄, Pd₆, and Pd₁₇) Water Oxidation Electrocatalysis. *ACS Nano* **2013**, *7*, 5808–5817.
- (122) Pearson, R. G. Recent Advances in the Concept of Hard and Soft Acids and Bases. *J. Chem. Educ.* **1987**, *64*, 561.
- (123) Pearson, R. G. Chemical Hardness and Density Functional Theory. *J. Chem. Sci.* **2005**, *117*, 369–377.
- (124) Parr, R. G.; Chattaraj, P. K. Principle of Maximum Hardness. *J. Am. Chem. Soc.* **1991**, *113*, 1854–1855.

- (125) Parr, R. G.; Pearson, R. G. Absolute Hardness: Companion Parameter to Absolute Electronegativity. *J. Am. Chem. Soc.* **1983**, *105*, 7512–7516.
- (126) Guzmán-Ramírez, G.; Aguilera-Granja, F.; Robles, J. DFT and GEGA Genetic Algorithm Optimized Structures of $\text{Cu}_n = \pm 1, 0, 2$; $n = 3-13$) Clusters. *Eur. Phys. J. D* **2010**, *57*, 49–60.
- (127) Tang, W.; Sanville, E.; Henkelman, G. A Grid-Based Bader Analysis Algorithm Without Lattice Bias. *J. Phys.: Condens. Matter* **2009**, *21*, 084204.

Graphical TOC Entry



Graphic.pdf